TECH LIBRARY KAFB, NM
0099892

NASA CONTRACTOR REPORT

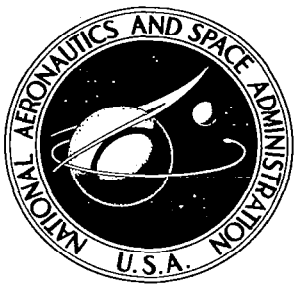

NASA CR-[illegible]
LOAN COPY RE
AFWL
KIRTLAND AFB, N

NASA CR-819

SEARCH FOR PLASMA OSCILLATIONS STIMULATED BY A PRE-BUNCHED ELECTRON BEAM FROM THE RENSSELAER LINEAR ACCELERATOR

by J. S. Mendell and E. H. Holt

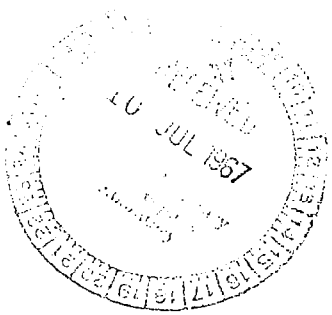

Prepared by
RENSSELAER POLYTECHNIC INSTITUTE
Troy, N. Y.
for

NATIONAL AERONAUTICS AND SPACE ADMINISTRATION • WASHINGTON, D. C. • JULY 1967

TECH LIBRARY KAFB, NM
0099892

NASA CR-819

SEARCH FOR PLASMA OSCILLATIONS STIMULATED BY A PRE-BUNCHED ELECTRON BEAM FROM THE RENSSELAER LINEAR ACCELERATOR

By J. S. Mendell and E. H. Holt

Distribution of this report is provided in the interest of information exchange. Responsibility for the contents resides in the author or organization that prepared it.

Issued by Originator as Technical Report No. 67-2

Prepared under Grant No. NsG-48 by
RENSSELAER POLYTECHNIC INSTITUTE
Troy, N.Y.

for

NATIONAL AERONAUTICS AND SPACE ADMINISTRATION

For sale by the Clearinghouse for Federal Scientific and Technical Information
Springfield, Virginia 22151 – CFSTI price $3.00

CONTENTS

SUMMARY	1
INTRODUCTION	1
HISTORICAL REVIEW	3
The Experiment of Merrill and Webb	3
The Experiment of Looney and Brown	4
The Experiments of Kojima, et. al.	6
The Experiment of Demirkhanov, et. al.	7
The Experiment of Kharchenko, et. al.	8
THEORETICAL ASPECTS	8
The Linac Electron Beam	9
The Stimulation of Plasma Oscillations	10
The Basic Equations	11
Modifying the Basic Equations	14
Calculation of Power Extracted from the Beam	17
Calculation of the Energy Stored in the Electric Fields	19
APPARATUS	22
The Time-Delay Circuit	23
The Experimental Vessel and the Plasma Pulser	23
The Combination Bridge and Receiver	25
PROCEDURE AND RESULTS	30
CONCLUSIONS	31
APPENDIX, HARMONIC ANALYSIS OF THE LINAC BEAM	33
REFERENCES	52

SEARCH FOR PLASMA OSCILLATIONS STIMULATED BY A PRE-BUNCHED ELECTRON BEAM FROM THE RENSSELAER LINEAR ACCELERATOR

by J. S. Mendell and E. H. Holt
Rensselaer Polytechnic Institute

SUMMARY

An experiment is described in which the electron beam from the R.P.I. Linear Accelerator was passed through an argon plasma to discover whether microwave oscillations could be detected outside the discharge vessel. As an experiment in plasma oscillations it is unique in the high energy of the beam and its pre-bunched nature. Because of resonance between the plasma frequency near the axis of the vessel and the sixteenth harmonic of the beam's fundamental frequency, the plasma electrons are expected to gain energy from the beam. The energy stored in the beam-plasma interaction region is expected to be high relative to the energy that the field of the beam would produce in free space. Some of this energy is expected to escape from the vessel in the form of microwave radiation. A special microwave bridge and receiver were constructed for the study of the radiation. According to an harmonic analysis of the Linac beam current, based upon an examination of the energy spectrum of the Linac, a peak beam current of 0.3 A contains a sixteenth harmonic component of about 0.1 A amplitude, whose frequency is the same order of magnitude as the plasma frequency. But this beam current passing through the discharge did not stimulate oscillations that could be detected with a K-band receiver placed outside the vessel. Taking into account the vessel-antenna geometry and the receiver sensitivity, it is concluded that any radiation produced by the beam was at a level lower than 0.4×10^{-10} watts per centimeter of plasma traversed.

INTRODUCTION

It has been predicted theoretically (ref. 1) and confirmed experimentally that an electron beam traversing a plasma stimulates radio frequency oscillations consisting of rarefactions and condensations of electron density. These oscillations occur at, or near, the plasma frequency. They may be strictly localized at some point along the beam (ref. 2), they may be standing plasma waves (ref. 3), or they may be traveling plasma waves (ref. 4). Oscillations have been detected in the sheaths which bound the plasma, including the cathode sheath in a diode and the accelerating anode in a discharge vessel employing an electron gun. They have been detected by inserting conducting probes into a discharge vessel and observing oscillations with the probes.

It is believed that an unmodulated electron beam cannot be responsible for oscillations. However, an initially unmodulated beam may acquire modulation

in passing through a plasma. There is evidence that an unmodulated beam of electrons becomes unstable in traversing a plasma and acquires a modulation at the plasma frequency, and there is also evidence that an unmodulated beam of electrons acquires a modulation in passing through oscillating sheaths. These two ways of acquiring modulation are not mutually exclusive, but the relative importance of the instability modulation and the sheath modulation is a very contentious point. Instability modulation (refs. 5,6) is thought to occur because the electron beam stimulates plasma waves, which propagate alongside the beam. Sheath modulation is believed to occur because there are oscillating electric fields in sheaths which modulate the velocity of the beam, causing density modulation at some point past the sheath. Both mechanisms depend upon the beam's passing through a long enough length of plasma to acquire a density modulation.

Analysis of plasma oscillations on the assumption that a gas discharge consists only of a plasma and a beam overlooks the fact that the external power source can contribute energy to the plasma. In order to discover whether oscillations could be produced with the bare essentials, a modulated beam and a quiescent plasma, it was decided to carry out beforehand one of the jobs the plasma accomplishes automatically: modulation of the beam at, or near, the plasma frequency. It was also decided to allow the plasma to decay so that any unsuspected processes depending on the utilization of external power sources would be inhibited.

The Linac is an accelerator which produces bunched beams of electrons of high enough energy to be unmodulated by the plasma. Furthermore, the Linac may inject its beam during the decay of the plasma, i.e., when the energy source has been disconnected and the electrode sheaths are disappearing. Passage of the Linac beam through a plasma vessel is expected to cause near-resonant oscillations of the plasma electrons. These oscillations are accompanied by strong electric fields, and the potential energy of these oscillating fields, plus the kinetic energy of the oscillating electrons, are much higher than the energy that the field of the beam would produce in free space. Electrons oscillating in a plasma vessel cause rf radiation which can be detected by an antenna placed outside the vessel or by probes in the plasma vessel itself. In this experiment radiation outside the vessel was sought, in order to avoid the use of plasma probes. There are several reasons for not using probes: (ref. 7)

i. Probes diminish the electron density in their neighborhood. This would be especially serious in a decaying plasma.

ii. Probes tend to acquire sheaths of net positive or negative charge. These are potential sources of spurious oscillations.

iii. Probes are connected to energized electronic circuits. This is contrary to the intention to remove all sources of power other than the Linac beam from the plasma.

iv. Passage of the Linac beam through the plasma would create an unusual environment for a probe. It is not clear how the probe would respond.

v. Since no previous investigators have used probes to detect oscillations in a decaying plasma there are no guidelines in seeking out and removing spurious effects. An example of a hypothetical spurious effect is the following: Since the plasma undergoes a pulse-and-decay cycle the receiver attached to a probe would see a constantly varying impedance which in itself might induce spontaneous oscillations in the amplifier.

To summarize, the object of the experiment was to stimulate plasma oscillations by passing a pre-bunched beam of electrons through an afterglow plasma and detect their presence by searching for microwave radiation outside the plasma vessel. This experiment has the following features:

a. The use of a decaying plasma eliminates the possibility that external power circuits furnish the power to maintain oscillations. All the power for oscillations must then come from the beam.

b. Since the plasma is allowed to decay, it approximates a "cold" plasma.

c. By the very nature of the accelerator, the beam is pre-modulated, so that sheath modulation or instability modulation by the plasma is not required. Conversely, the beam electrons move with almost the speed of light, so that additional modulation of the beam density cannot be caused by any oscillating fields in the plasma. Furthermore, the beam is not injected through an energized electrode, as in the Looney-Brown (1954) experiment (ref. 3) or as in any other experiment using a separate electron gun.

d. The beam may be injected into the plasma in 0.1 μ sec bursts at any pre-selected time during the plasma decay period. During this period the plasma density decays by about 1/100 of 1%. Also, because the high energy electrons have a very small tendency to ionize the argon gas, the beam does not inhibit the decay of the plasma.

e. Probes are not inserted into the beam-plasma interaction region.

HISTORICAL REVIEW

The Experiment of Merrill and Webb

Using the vessel shown in Figure 1, Merrill and Webb (ref. 2) studied the relationship between break-up of an unmodulated electron beam and the appearance of plasma oscillations. An arc was struck between the cathode and the anode of a vessel containing mercury vapor at 0.003 torr. The arc current was between 20 mA (for an 11.7 V arc drop) and 50 mA (for a 14.7 V arc drop). The probe was employed to measure the electron density of the arc, to measure the electron velocity distribution of the arc, and to detect oscillations in the region between cathode and anode. When the probe was used to detect oscillations it was connected to a crystal rectifier and to a Lecher wire system. The rectified crystal current was a measure of the oscillation strength, and the distance between nodes on the Lecher wires was a measure of frequency.

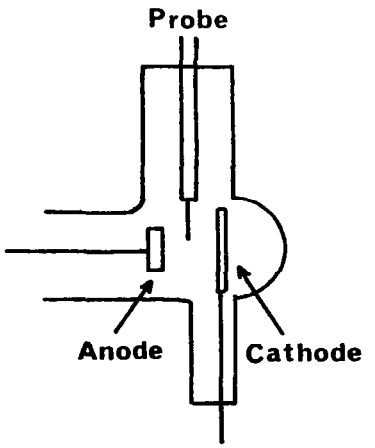

The experiment of Merrill and Webb to study plasma oscillations in an unmodulated electron beam.

Figure 1

Merrill and Webb moved the probe through the 15 mm distance between the electrodes. They discovered that the electron temperature was about 30,000 ^{o}K throughout this region, the electron density was 2-4 x 10^{10}/cm^{3}, and

the distribution of velocities was approximately Maxwellian. The probes also revealed the presence of electrons whose energy was much greater than the arc drop voltage. The stream of electrons whose energy was determined by the arc drop voltage were called primaries. In moving the probe from cathode to anode in 0.2 mm steps Merrill and Webb found two regions in which scattering of the primary beam occurred, and two regions in which oscillations at the plasma frequency occurred. For example, when the arc drop was 11.7 V and the arc current was 20 mA, all primaries had the same energy up to a point 4.3 mm from the cathode. But in the region between 4.3 mm and 4.5 mm scattering occurred and electrons appeared in the beam with energies up to 26 V. In the region between 5.3 mm and 6.0 mm, oscillations at the plasma frequency, 1.2×10^9 cps, were detected. Again, at 6.1 mm, a region of scattering was detected in which primary electrons acquired additional energy. At 6.8 mm oscillations at the plasma frequency were detected. (Merrill and Webb have not stated the length in millimeters of the second region of scattering and oscillation.)

They concluded that the oscillations detected at 5.3 mm and 6.8 mm were due to velocity modulation of the primary electron beam at 4.3 mm and 6.1 mm and that these oscillations occurred in the regions in which velocity modulation was translated into density modulation, that is, rarefactions and condensations of electron density. They also concluded that the scattering of primary electrons at 4.3 mm and 6.1 mm was due to strong oscillating electric fields at these points, although these fields could not be directly detected by probes. They were unable to explain why the oscillations were localized fields rather than propagating plasma waves or standing waves. Nor were they able to explain the mechanism that energized the oscillations.

The experiment illustrates the reciprocal interaction between a plasma and a low energy beam. The beam causes oscillations and the oscillations modulate the beam.

The Experiment of Looney and Brown

Looney and Brown (ref. 3) pointed out that the use of electrons from the cathode region of an arc to study plasma oscillations has several disadvantages. One is the fact that the plasma density and temperature are controlled by the energy and density of the beam electrons. Another is the fact that the beam electron energy and density are difficult to control. They constructed a discharge vessel which employed a set of electrodes to create an arc in mercury vapor (at 0.003 torr), and also an electron gun to inject a beam of fast electrons into the arc. Figure 2 shows the arrangement of electrodes in the vessel. The distance between the accelerating anode and the collector is 15 mm. An arc was struck between the cathodes and the wire anodes. This arc created a plasma in the region between A and D. The plasma density, which was $3\text{-}14 \times 10^9/cm^3$, depended upon the arc current. The anode marked gun anode is the anode of a discharge which is generated in a sidearm of the tube. Electrons from this discharge escaped through a 1 mm hole in the gun anode and were accelerated through several hundred volts potential as they proceeded to the accelerating anode. Some of them passed through a 1 mm hole this electrode and drifted through the plasma region to the collector. The accelerating anode and the collector could be biased negatively with respect to the wire anodes, through a range of 200 volts. Increasing the negative bias or increasing the electron density of the arc increased the thickness of the

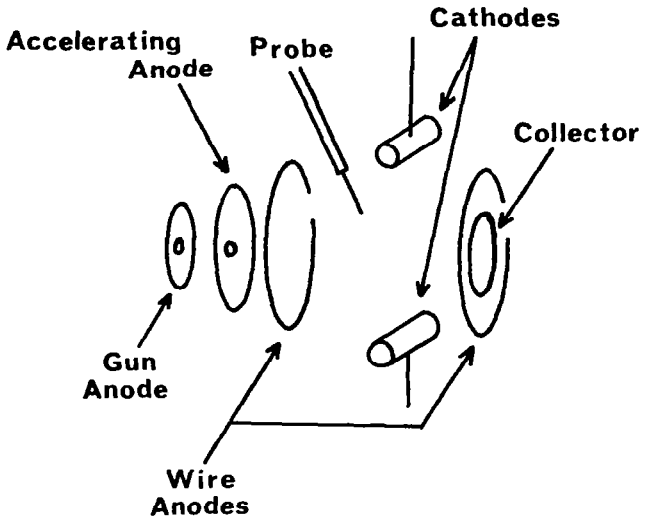

The experiment of Looney and Brown using an independent beam of fast electrons.

Figure 2

sheaths on the accelerating anode and the collector.

The experiment consisted of measuring the standing wave pattern of oscillations in the plasma as a function of sheath thickness. When there were thick sheaths, a movable probe connected to a superheterodyne receiver (of unspecified sensitivity) detected oscillations in a frequency band near the plasma frequency (760 to 820 Mcs). Moving the probe throughout the plasma showed that the region between the sheaths exhibited an oscillating standing wave. Because the sheath edges were visible, it was possible to establish that the standing wave pattern was contained in the region between them. It was found that increasing the sheath thickness squeezed the standing wave pattern into a smaller region. This is shown in Figure 3. For example in parts (i) and (ii), when the electron density in the discharge increased, and the sheath thickness increased, the frequency of the oscillations increased. This increase in frequency maintained the standing wave pattern of four "loops". The standing wave pattern responded to stronger squeezing by changing to a different pattern with fewer "loops" between the sheaths. Again in Figure 3, parts (ii) and (iii) show that when the electron density of the discharge was increased sufficiently, the frequency of the oscillations decreased abruptly, removing one "loop" from the standing wave pattern.

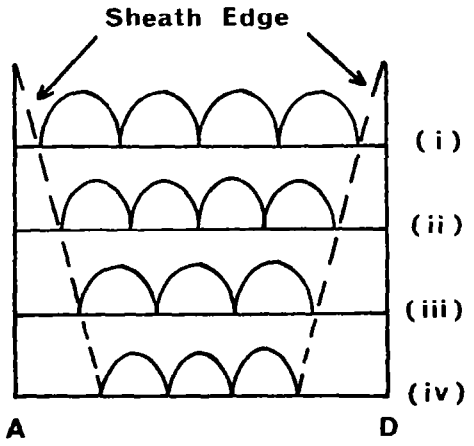

Standing wave pattern of Looney and Brown showing how the wavelength of the standing waves decreases with increasing electron density.

Figure 3

Merrill and Webb had found that the oscillation frequency was determined by the density of electrons in the plasma and smoothly followed increases and decreases of density. However, Looney and Brown found that the frequency of oscillations depend upon the changes in standing wave pattern, and exhibited abrupt changes as the number of "loops" in the standing wave pattern changed. They therefore assumed that there were strong oscillating fields in the sheaths, whose frequency was forced to remain in the neighborhood of the plasma frequency. The fields in the sheath on the accelerating anode were assumed to velocity modulate the electron beam at a point near the sheath edge

of the plasma. As the beam crossed the plasma its velocity modulation caused the electrons to bunch. The oscillating fields in the sheath on the collector retarded the bunches, extracting energy, and increasing the amplitude of sheath oscillations.

According to this model the sheaths acquire radio frequency power at the expense of the d.c. power in the beam. The sheaths modulate the beam, making possible the stimulation of longitudinal standing waves in the plasma. The proper phase relation between the electric field at the point where the beam is modulated and the electric field at the point where the energy is extracted requires that the average transit time of a beam electron across the distance x between edges is

$$\frac{x}{\mu} = \frac{4k+1}{4} \frac{1}{f}$$

where $k = 0, 1, 2, \ldots,$ and μ is the velocity of the beam electrons. This formula shows that when the distance x is decreased, either f, the frequency of oscillations, or the number of "loops" between sheaths, must change.

This experiment is an important example of the critical part played by sheaths in determining the frequency of oscillations. It indicates that sheaths are capable of modulating an electron beam as it enters a plasma, and perhaps participating in transit-time effects of the sort found in klystrons.

The Experiments of Kojima, et al.

Kojima, et al. (ref. 4) constructed the mercury arc diode shown in Figure 4. They inserted probes into the plasma region and detected oscillations near the plasma frequency (1 kMc). Then they used a Yagi antenna to search for radio oscillations outside the vessel. The oscillations that they detected outside the vessel occurred at the same frequency as the oscillations they detected inside the vessel. This was taken as evidence that the electrons oscillating inside the vessel were causing radiation outside. The radiation was most intense at right angles to the axis of the vessel.

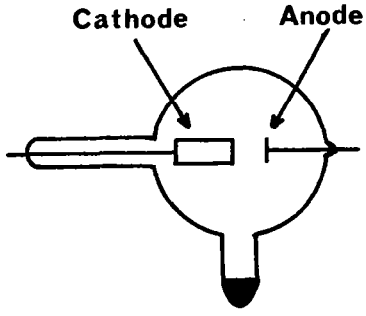

The cell used by Kojima et al. to detect plasma oscillations by measurement of radiation from the plasma.

Figure 4

In a later experiment they constructed a cylindrical discharge vessel, filled with mercury vapor at a pressure of 0.003 torr, and discovered radiation outside the vessel due to plasma oscillations inside. The radiation was detected with a microwave horn that was pointed at right angles to the axis of discharge vessel and intercepted about 1/100 of the radiation emitted by the vessel. The radiation was uniformly intense along the whole positive column of the discharge. The radiation was concentrated in a 40 Mcs bandwidth about the plasma frequency. The power in this bandwidth received by the horn was 2×10^{-10} watts, so the total power emerging from the vessel was 2×10^{-8} watts. The discharge operated at 0.9 A and 47 V, for an input power of 42 watts, hence

the coupling between the dc input and the rf output was 2×10^{-8} watts/40 watts = 0.5×10^{-9}, or 93 db. Since no estimate was made of the power level of the rf plasma oscillations inside the vessel, there is no measure of the coupling between these oscillations and the radiation power.

The Experiment of Demirkhanov, et al.

Demirkhanov, et al. (ref. 8) employed a vessel resembling that of Looney and Brown and injected a beam of 3 kv electrons into a plasma. Their vessel contained a set of electrodes which was used to generate a plasma with an electron density of about 10^{11} cm^{-3}, and employed an electron gun mounted in a sidearm to inject a beam of 0.4 - 2.0 amp. into the plasma. They did not state the dimensions of their vessel. Experiments were performed in argon, hydrogen and nitrogen at pressures of 0.01 - 0.001 torr. The results are not ascribed to any particular gas or pressure, implying that they were independent of these parameters.

A receiver was connected to a probe (to measure oscillations inside the vessel), or an antenna (to measure radiation outside the vessel). The experiment consisted of setting the receiver to some frequency in the range 1.8 kMc to 3.2 kMc and observing its peak response as the electron density of the plasma was varied. Figure 5 shows that the receiver response is greatest when the receiver is tuned to the plasma frequency for both the probe and the antenna.

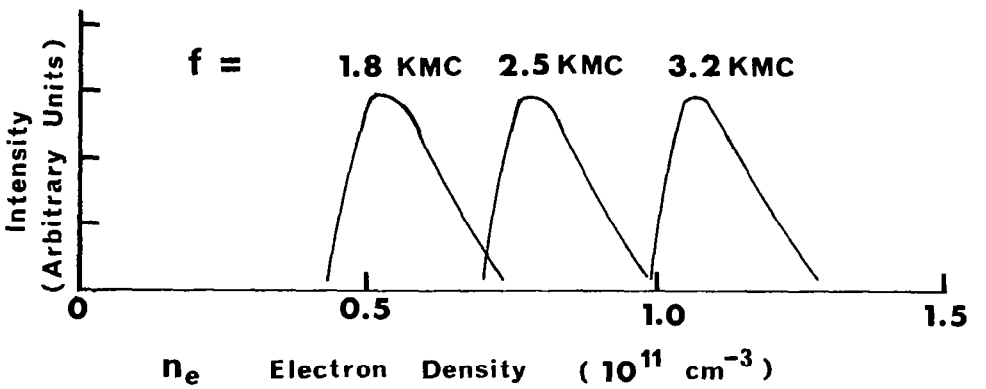

The results of Demirkhanov et al. Receiver output intensity is plotted as a function of plasma electron density. Both probe and radiation measurements gave similar results.

Figure 5

The receiver sensitivity was given as 10^{-12} watts. No information was given about the size or position of the antenna, but if it is assumed that the antenna intercepts 1/100 of the radiation escaping from the vessel, and that the signal is 10 db above bare detectability, then the output radiation is at a level of at least 10^{-9} watts. Since the input power is about 1 amp. x 3000 volts = 3000 watts, the coupling between the d.c. input power and the rf radiation is $1/3 \times 10^{-12}$, or - 125 db.

The Experiment of Kharchenko, et al.

Kharchenko, et al. (ref. 5) passed an 80 kV, 1 amp. electron beam through a plasma created by an rf oscillator. They varied the plasma electron density in the range 10^{11} cm^{-3} by varying the plate voltage of the rf oscillator. The electron completely filled a plasma region 3.65 mm in diameter and either 10 cm or 20 cm long. Their experiment consisted, in part, of studying the effect of the plasma path length in modulating the beam. They stated that the gas pressure was 0.001 torr, but did not state what gas they used.

The electron beam passed through the plasma and then through a tunable resonant cavity, which was employed to determine whether the beam had been modulated (bunched). The cavity could be excited by a beam modulated at its resonant frequency. Part of the resonator's energy was coupled out to a crystal detector. The electron density was measured by tuning the resonator to a certain frequency and increasing plasma density until the crystal current peaked. This is exactly analogous to the procedure of Demirkhanov, et al., and gave curves of electron density vs. crystal current that strongly resemble the curves of Figure 5. They found that passing a beam through 20 cm of plasma induced modulation at (or near) the plasma frequency, while passing the beam through 10 cm of plasma did not induce modulation. They also found that initial modulation of the beam resulted in amplification of the modulation, even in a 10 cm plasma path length.

This experiment shows the importance of a small amount of pre-modulation in causing bunching of a beam. It is well known that thick sheaths play a critical part in causing plasma oscillations, but thin sheaths, with relatively weak oscillating fields, may also be capable of furnishing the small amount of pre-modulation that leads to instability.

THEORETICAL ASPECTS

Two conditions must exist for the Linac beam to cause rf radiation that can be detected outside an experimental vessel.

1. The beam must set up electron oscillations within the beam-plasma interaction region.

2. Some of the rf energy within the interaction region must escape from the vessel.

The first condition can be analyzed theoretically, but not with great precision. Not all conditions existing in the beam-plasma interaction region are experimentally controllable, and this affects the strength of the interaction. For instance, the electron temperature and the homogeneity of the plasma cannot be controlled. The second point does not lend itself to simple theoretical analysis, although there is strong evidence from the experiments of Kojima and of Demirkhanov that some energy is converted into radiation at the plasma frequency. We will show here that the Linac beam is expected to stimulate plasma electron oscillations, building up high electric fields within the vessel. The energy density associated with the fields is estimated in an order of magnitude calculation, and it is then pointed out that if a small fraction of this energy is radiated it should be detected outside the vessel by the sensitive receiver used.

The Linac Electron Beam

For reasons explained in Appendix A, bunches of electrons from the R.P.I. Linac constitute a beam current which may be resolved into a dc current and an infinite number of rf currents. According to Fourier analysis these rf currents have frequencies of 1.3 kMc and its integral multiples so that the beam should be able to excite resonators tuned to 1.3 kMc, 2.6 kMc, ..., 20.8 kMc, ..., etc.

It will be shown in the following sections that the electrons in the plasma, which acts as a target for the Linac beam, can resonate at frequencies in the neighborhood of the sixteenth harmonic if the proper electron density is present. It turns out that the plasma is expected to interact with the sixteenth harmonic but scarcely interact with higher or lower harmonics. Therefore, in setting up the calculation of the interactions, the higher and lower frequency rf currents may be ignored. It is simply assumed that the source (the forcing term) varies as $\exp(-i\omega t)$, which permits the convenient substitution $\partial/\partial t = -i\omega$ throughout the calculations.

The Fourier analysis of the electron beam is discussed in detail in Appendix A. It is shown that the charge density can be written

$$\rho\left(t - \frac{z}{v_b}\right) = \frac{q}{\pi a^2 v_b T} \sum_{N=-\infty}^{\infty} \eta_N \exp(i\omega_N (z - v_b t)/v_b) \qquad (1)$$

where q is the charge of a single bunch of electrons, πa^2 is the cross-sectional area of a bunch, $v_b T$ is the distance between bunches, and η_N is a complex coefficient. The average charge density for the sixteenth harmonic is

$$\langle \rho_{16} \rangle = \frac{q}{\pi a^2 v_b T} \eta_{16} \exp(i\omega_{16}(z - v_b t)/v_b) \qquad (2)$$

When the peak beam current is 0.3 A,

$$q = \frac{0.3}{1.3 \times 109} = 2.3 \times 10^{-10} \quad \text{coulomb.}$$

Also $\pi a^2 = 2 \times 10^{-4} (\text{meter})^2$ and $v_b T = 0.23 (\text{meter})$ and from the analysis of Appendix A, $\eta_{16} = 0.3$ so that

$$\langle \rho_{16} \rangle = 1.5 \times 10^{-6} \text{ coulomb/m}^3 \qquad (3)$$

Equations 1, 2, and 3 are correct when the transverse profile of the charge density of the beam is uniform. Actually, the transverse profile of the charge density is not uniform, but is a decreasing function of radius. A rough measurement of the density profile (ref. 9) indicates that the profile is bell-shaped. But, in the numerical calculations here, it is assumed that the beam is uniform, and the average charge density is used.

The Stimulation of Plasma Oscillations

Plasma frequency and collision frequency - A 60 μsec spike of current is applied to the argon gas in the discharge vessel by a dc pulser, producing an ionized column of gas 28 cm long and 5 cm in diameter. At the instant the ionizing energy is removed the plasma electron density is at least $10^{13}/cm^3$, and the electron temperature is probably 10,000 - 30,000 °K, which means that the rms velocity of plasma electrons is 5-10 x 10^7 cm/sec.

This plasma lasts only a few milliseconds. The interval in which there remains appreciable ionization is known as the afterglow. During the afterglow the plasma electron temperature and the electron density decrease. The temperature falls because the electrons lose energy in collisions with gas atoms. The electron density falls because of ambipolar diffusion of the charged particles to the walls of the vessel. This diffusion not only diminishes the electron density but causes a non-uniformity of electron density. The radial distribution of electron density persisting longest in the afterglow is given by the expression

$$n_o = (n_o)_{axis} J_o(2.4 \frac{r}{a})$$

where J_o is the zero-order Bessel function, and a is the radius of the plasma column.

A lower limit to the collision frequency can be estimated in the following way. Because of the Ramsauer effect the electron-argon atom collision cross-section is small in the energy range below one electron volt and at 0.7 ev (corresponding to an electron temperature of about 9000°K) the collision cross-section is a minimum. According to the data given by Brown and Allis (ref. 10) at 0.7 ev the electron mean free path in argon at 0.10 torr is 100 cm, which makes the collision frequency 0.3 Mc. At an electron temperature slightly above or below 9000°K the collision frequency will be larger.

Plasma electrons have a natural frequency of oscillation, known as the plasma frequency which is a function of the plasma density. Roughly, the plasma frequency is given by the expression

$$f_p = 10^4 \, n_o^{1/2} \qquad (4)$$

where f_p is in cps and n_o is the number of electrons/cm^3.

The condition of near-resonance - When the plasma density in some region of the discharge vessel is 5 x $10^{12}/cm^3$ the plasma frequency there is close to the sixteenth harmonic frequency of the Linac beam. When the beam passes through this region it is expected to set the plasma electrons into near-resonant oscillation, which results in an intensification of the electric fields (over their free space values). Relatively large energy densities should build up in the beam-plasma interaction region because of the intense electric fields and the high kinetic energy of the oscillating electrons. The oscillations will be weakly damped because of collisions between the electrons and the argon atoms, but the beam should supply power to maintain the oscillation.

Since the plasma is decaying, at some instant in the afterglow every small region near the center of the vessel attains a plasma frequency equal to the sixteenth harmonic frequency. However, these instants occur at different times in different regions, because the plasma is not uniform. It is contrived in designing the experiment to fire the beam through the vessel when the plasma frequency in the center of the vessel is very close to the sixteenth harmonic.

The permittivity of the plasma is $\epsilon_o \epsilon_r$, where ϵ_r is called the dielectric coefficient, and the electric fields in the plasma are proportional to ϵ_r^{-1}. The conditions encountered experimentally (and explained in later sections) justify the approximation

$$\epsilon_r \approx \frac{2\Delta\omega}{\omega_p} + i\,\frac{\nu}{\omega_p} \tag{5}$$

where $\omega_p = 2\pi f_p$, $\omega = 2\pi(f-f_p)$, f is the sixteenth harmonic frequency, and ν is the collision frequency. The smaller the absolute value of ϵ_r, the greater the fields. The absolute value of ϵ_r cannot be reduced beyond ν/ω_p no matter how close the frequencies are to equality. But, if the value of $2\Delta\omega/\omega_p$ is much greater than ν/ω_p the fields are limited by the deviation from resonance. Also, since $\Delta\omega = \omega-\omega_p$, and since ω_p is a function of the plasma density, in a non-uniform region of plasma density the dielectric coefficient is also non-uniform.

The cross-sectional radius of the Linac beam is 0.8 cm. According to equations 3 and 4, the plasma density 0.8 cm from the axis of the vessel is 0.85 of the axial density, which means that the plasma frequency 0.8 cm from the axis is 0.9 of the axial plasma frequency. As a consequence of this ten percent change within the beam-plasma interaction region, the dielectric coefficient ranges over several orders of magnitude, between 10^{-3} and unity. In the neighborhood where the coefficient is 10^{-3} the beam sets up strong electric fields and furnishes considerable power to the oscillations; in the region where the coefficient is close to unity the beam builds up fields scarcely different from those that would exist in free space and furnishes very little power to the oscillations. In the steady state the average power P supplied by the beam (of current density J) to the oscillations of the electric field E is described by the expression

$$P = \frac{1}{2} R_e \int \bar{E} \cdot \bar{J}^* \, dv \tag{6}$$

where dv is a volume element of the interaction region. Because ϵ_r is complex $\bar{E} \cdot \bar{J}^*$ has a real part. Of course, the integrand varies over the region of integration, and this point will be discussed in a later section.

The Basic Equations

The six basic equations that describe the behavior of our plasma are the four Maxwell's equations, the equation of continuity of electron charge, and the electron force equation. These equations will be explained in this section. In the following section certain simplifications permitted by the experimental conditions will be made.

The Maxwell's equations for a plasma traversed by an electron beam are equations 7 - 10 below.

$$\bar{\nabla} \times \bar{E} = - \mu_o \frac{\partial \bar{H}}{\partial t} \tag{7}$$

$$\bar{\nabla} \times \bar{H} = \epsilon_o \frac{\partial \bar{E}}{\partial t} - ne\bar{v} + \rho_s \bar{v}_b \tag{8}$$

$$\bar{\nabla} \cdot \bar{E} = \frac{1}{\epsilon_o}(-ne + n_i e + \rho_s) \tag{9}$$

$$\bar{\nabla} \cdot \bar{H} = 0 \tag{10}$$

where $\bar{v}_b$ is the beam electron velocity

ρ_s is the beam charge density

$\bar{v}$ is the systematic velocity of the oscillating plasma electrons

m is the rest mass of a plasma electron

n is the plasma electron density

n_i is the plasma ion density.

The equation of continuity of the plasma electronic charge is the expression

$$\bar{\nabla} \cdot (n\bar{v}) + \frac{\partial n}{\partial t} = 0 \tag{11}$$

and the force equation for a plasma electron is the expression

$$m \frac{\partial \bar{v}}{\partial t} + m \bar{v} \cdot \bar{\nabla} \bar{v} = -e\bar{E} - \frac{kT_e}{m} \bar{\nabla} n - m\nu\bar{v} \tag{12}$$

where T_e is the plasma electron temperature, and k is Boltzmann's constant.

The total charge density in equation 9 is the sum of the densities due to the plasma electrons, the ions, and the beam electrons. However the ions do not contribute to the current density in equation 8 because they are almost stationary compared with the electrons.

The left-hand side of equation 12 is the rate of change of momentum, $m\, d\bar{v}/dt$. The first term on the right-hand side is the electrical force, and the second term on the right-hand side is the force due to pressure gradients. (ref. 11). The third term on the right-hand side is the rate at which systematic electronic motion is randomized. That is, since mv is the electron momentum, and since ν is the number of randomizing collisions per unit time, $m\nu\bar{v}$ is the average rate of change of momentum due to collisions.

The passage of the electron beam through the plasma sets up oscillations. These oscillations are not only characterized by electric fields, $\bar{E}$, and magnetic fields, $\bar{H}$, but by electron density rarefactions and condensations, n_1, and electron velocities, $\bar{v}$. Thus the total electron density consists of two parts: an ambient density, n_o, and rarefactions or condensations due to the oscillation, n_1.

The variables are divided into zero-order, first-order, and second-order terms. Zero-order terms are n_o, n_i, T_e, plus all of the physical constants and the differential operators. (In other words, the terms that do not disappear when the beam is turned off.) The first-order terms are ρ_s, $\bar{v}_b$, $\bar{E}$, $\bar{H}$, $\bar{v}$, n_1, and the products of any one of these with a zero-order term. Second-order terms are the products of two first-order terms. The substitution $n = n_o + n_1$ is made in equations 7-12 and first-order terms are collected, yielding the linearized equations:

$$\bar{\nabla} \times \bar{E} = - \mu_o \frac{\partial \bar{H}}{\partial t} \tag{13}$$

$$\bar{\nabla} \times \bar{H} = - n_o e \bar{v} + \epsilon_o \frac{\partial \bar{E}}{\partial t} + \rho_s \bar{v}_b \tag{14}$$

$$\bar{\nabla} \cdot \bar{E} = - \frac{1}{\epsilon_o} (e n_1 - \rho_s) \tag{15}$$

$$\bar{\nabla} \cdot \bar{H} = 0 \tag{16}$$

$$\bar{\nabla} \cdot (n_o \bar{v}) = - \frac{\partial n_1}{\partial t} \tag{17}$$

$$- m \frac{\partial \bar{v}}{\partial t} = e \bar{E} + \frac{1}{n_o} \bar{\nabla} (k T_e n_1) + m \nu \bar{v} \tag{18}$$

When all first-order terms vary as $\exp(-i\omega t)$, the equations lead to the expressions below.

$$\bar{\nabla} \times \bar{E} = i \omega \mu_o \bar{H} \tag{19}$$

$$\bar{\nabla} \times \bar{H} = - n_o e \bar{v} - i \omega \epsilon_o \bar{E} + \rho_s \bar{v}_b \tag{20}$$

$$\bar{\nabla} \cdot \bar{E} = - \frac{1}{\epsilon_o} (e n_1 - \rho_s) \tag{21}$$

$$\bar{\nabla} \cdot \bar{H} = 0 \tag{22}$$

$$\bar{\nabla} \cdot (n_o \bar{v}) = i\omega n_1 \tag{23}$$

$$i\omega m Y \bar{v} = e\bar{E} + \frac{1}{n_o} \bar{\nabla} (kT_e n_1) \tag{24}$$

where $Y = 1 + i \frac{\nu}{\omega}$

Modifying the Basic Equations

In this section it will be shown that under certain circumstances (for a "cold" plasma) the plasma has an effective dielectric coefficient whose use simplifies the form of the Maxwell's equations.

The equation of continuity - Equation 17 may be rewritten:

$$(\bar{\nabla} n_o) \cdot \bar{v} + n_o \bar{\nabla} \cdot \bar{v} = i\omega n_1 \tag{25}$$

The magnitude of the first term on the left is approximately $n_o v/a$, where a is the radius of the plasma column. The magnitude of the second term is approximately $\omega n_o v/v_b$, where the factor ω/v_b arises in the following way: The sixteenth harmonic current of the Linac beam looks like

$$\bar{J}_{16} = \rho_{16} v_b \exp i\omega(z - v_b t)/v_b \tag{26}$$

so that the waves set up by this current vary as $\exp(i\omega a/v_b)$. Hence

$$\left| \bar{\nabla} n_1 \right| \approx \frac{\omega}{v_b} n_1$$

The ratio of the first term to the second is

$$\frac{v_b}{\omega a} = \frac{3 \times 10^{10} \text{ cm/sec}}{2\pi \times 20.8 \times 10^9/\text{sec} \times 2.5 \text{ cm}} \approx \frac{1}{10}$$

so that

$$n_o \bar{\nabla} \cdot \bar{v} = i\omega n_1 \tag{27}$$

The plasma frequency and the dielectric constant - At this point it is convenient to define two new quantities. The plasma frequency (in radians per second) is defined by

$$\omega_p = (n_o e^2/\epsilon_o m)^{1/2} \tag{28}$$

and the dielectric constant is defined by

$$\epsilon_r = 1 - \frac{\omega_p^2}{\omega^2 Y} = \frac{\omega^2 - \omega_p^2 + i\nu\omega}{\omega^2(1+i\nu/\omega)} \tag{29}$$

Now $\nu \ll \omega$ and when $\omega - \omega_p (= \Delta\omega) \ll \omega$ we can write,

$$\epsilon_r \approx \frac{2\omega}{\omega_p} + i\frac{\nu}{\omega_p} \tag{30}$$

Significance of the dielectric coefficient - Taking the divergence of equation 24, we get the expression

$$i\omega Y \bar{\nabla}.\bar{v} = \frac{e}{m}\bar{\nabla}.\bar{E} + \frac{1}{n_o}\frac{kT_e}{m}\nabla^2 n_1 \tag{31}$$

Using equations 21 and 27 to eliminate $\bar{E}$ and $\bar{v}$ we get the expression

$$\frac{kT_e}{m}\nabla^2 n_1 + \omega^2 Y \epsilon_r n_1 = -\frac{1}{e}\omega_p^2 \rho_s \tag{32}$$

The first term on the left is of magnitude

$$\frac{kT_e}{m}\frac{\omega^2}{v_b^2} n_1$$

The ratio of the magnitude of the first term to the magnitude of the second term is the expression

$$\frac{kT_e}{m}\frac{1}{v_b^2}\frac{1}{|Y|}\frac{1}{|\epsilon_r|} \approx \frac{kT_e}{m}\frac{1}{v_b^2}\frac{\omega_p}{\left[4(\Delta\omega)^2 + Y^2\right]^{1/2}} \tag{33}$$

In the early afterglow, when T_e is about 3000°, $\nu = 0.3 \times 10^6$/sec, $(3kT_e/m)^{1/2} = 10^7$ cm/sec and $\omega_p = 10^{11}$/sec. So, the ratio of the two terms is

$$\frac{10^{14}}{10^{21}} \times \frac{10^{11}}{\left[4(\Delta\omega)^2 + (0.3 \times 10^6)^2\right]^{1/2}}$$

Since we are interested in the situation for which $\Delta\omega = 2\pi \times 20$ Mcs $= 10^8$/sec, the ratio is quite small and equation 29 becomes the expression

$$n_1 = -\frac{\omega_p^2}{\omega^2}\frac{1}{Y\epsilon_r}\frac{\rho_s}{e} \tag{34}$$

Equation 31 may be used to eliminate n_1 from equation 18, yielding the expression

$$\bar{\nabla}.\bar{E} = -\frac{1}{\epsilon_o \epsilon_r} \rho_s \tag{35}$$

Using equation 24 to eliminate $\bar{v}$ from equation 20, we obtain

$$\bar{\nabla} \times \bar{H} + i\omega\epsilon_o\epsilon_r\bar{E} = \bar{J}_1 + \bar{J}_2 \tag{36}$$

where

$$\bar{J}_1 = -\frac{kT_e}{m}\frac{e}{i\omega Y}\bar{\nabla} n_1 \tag{37}$$

$$\bar{J}_2 = \rho_s \bar{v}_b \tag{38}$$

Now

$$\frac{|\bar{J}_1|}{|\bar{J}_2|} = \frac{\frac{kT_e}{m}\frac{e}{i\omega Y}\bar{\nabla} n_1}{\rho_s v_b} = \frac{\frac{kT_e}{m}\frac{e}{\omega}\frac{\omega}{v_b} n_1}{\rho_s v_b} \tag{39}$$

Using equation 34 to express n_1 in terms of ρ_s we obtain

$$\frac{|\bar{J}_1|}{|\bar{J}_2|} = \frac{kT_e}{m}\frac{1}{v_b^2}\frac{\omega_p^2}{\omega^2}\frac{1}{\epsilon_r} \approx \frac{kT_e}{m}\frac{1}{v_b^2}\frac{\omega_p}{2\Delta\omega} \tag{40}$$

So that

$$\frac{|\bar{J}_1|}{|\bar{J}_2|} \ll 1$$

Hence, equation 36 becomes the expression

$$\bar{\nabla} \times \bar{H} = -i\omega\epsilon_o\epsilon_r\bar{E} + \rho_s\bar{v}_b \tag{41}$$

To summarize, the Maxwell's equations in the plasma can be written as equations 42 - 45 below

$$\bar{\nabla} \times \bar{H} = -i\omega\epsilon_o\epsilon_r\bar{E} + \rho_s\bar{v}_b \tag{42}$$

$$\bar{\nabla} \times \bar{E} = i\omega\mu_o\bar{H} \tag{43}$$

$$\bar{\nabla} \cdot \bar{E} = \frac{1}{\epsilon_o\epsilon_r}\rho_s \tag{44}$$

$$\bar{\nabla} \cdot \bar{H} = 0$$

providing that it is valid to write

$$\frac{kT_e}{m} \frac{1}{v_b^2} \ll \frac{\Delta f}{f_p}$$

That is, they are correct when the signal frequency (the sixteenth harmonic) is not too close to resonance.

These equations have the same form as the Maxwell's equations in free space, except for the effective dielectric permittivity, $\epsilon_o \epsilon_r$. This means that the presence of the plasma increases the electric field of the beam by ϵ_r^{-1}. The phase velocity of electromagnetic waves in a plasma is given by the expression

$$v_{ph} = (\epsilon_o \epsilon_r \mu_o)^{-1/2} = c\epsilon_r^{-1/2} \tag{46}$$

so that $\epsilon_r^{1/2}$ is the complex index of refraction.

Calculation of Power Extracted from the Beam--Steady State Behavior

From equation 42 we obtain

$$\bar{E} = \frac{1}{-i\omega\epsilon_o \epsilon_r} \bar{\nabla} \times \bar{H} + \frac{1}{i\omega\epsilon_o \epsilon_r} \rho_s \bar{v}_b \tag{47}$$

The first term on the right-hand side is the electric field due to the curl of the magnetic field set up by the beam. To solve for this term would involve setting up the difficult boundary value problem for the electric and magnetic fields stimulated by a beam traversing a non-uniform plasma. The second term, however, depends on the beam charge density and the plasma density where the beam passes through the plasma. Considering only the second term, which will be called $\bar{E}'$, equation 47 becomes

$$\bar{E}' = \frac{1}{i\omega\epsilon_o \epsilon_r} \rho_s \bar{v}_b = \frac{1}{i\omega\epsilon_o \epsilon_r} \bar{J}_s \tag{48}$$

When the Linac beam is turned on it sets up plasma electron oscillations. These are the superposition of two oscillations at pure frequencies; there is a damped transient oscillation at the plasma frequency and a forced oscillation at the sixteenth harmonic frequency.

Now the collision frequency is in the order of 0.3 Mc - 1.0 Mc. The transient oscillations at the plasma frequency that occur when the Linac beam is turned on will persist for several periods of collision, so that the time

required for the establishment of the steady state is of the order of 3 - 10 μsec. Since the length of an electron burst from the Linac is only 0.1 μsec, it is not expected that the steady state will be established in this short time. Nevertheless, the steady state behavior can be calculated as a limiting example of what might occur if the beam were left on long enough.

In the steady state the average power delivered by the beam to the plasma is given by the expression

$$P = \frac{1}{2} R_e \int \bar{E} \cdot \bar{J}^* dv \tag{49}$$

where the integral is taken over the interaction region, i.e., the region traversed by the beam. The length of this region is the length of the vessel, 28 cm, and the diameter of this (cylindrical) region is the diameter of the beam, 1.6 cm, for a total volume of 50 cm^3. Within this region the integrand is a function of position. Firstly, the current density of the Linac beam is a decreasing function of distance from the axis. Secondly, the plasma frequency is a decreasing function of distance from the axis, so that ϵ_r is not uniform.

Substituting equation 30 in equation 48 gives the expressions

$$\bar{E}' = \frac{1/\epsilon_o}{-\nu + 2i\Delta\omega} \bar{J}_s \tag{50}$$

$$= \frac{1}{\epsilon_o} \frac{-\nu - 2i\Delta\omega}{\nu^2 + 4(\Delta\omega)^2} \bar{J}_s \tag{51}$$

so that we have

$$\bar{E}' \cdot \bar{J}^* = \frac{1}{\epsilon_o} \frac{-\nu + 2i\Delta\omega}{2 + 4(\Delta\omega)^2} |J|^2 \tag{52}$$

and

$$\frac{1}{2} R_e(\bar{E}' \cdot \bar{J}^*) = -\frac{1}{2} \frac{1}{\epsilon_o} \frac{\nu}{\nu^2 + 4(\Delta\omega)^2} |J|^2 \tag{53}$$

The integrand of equation 49 has its largest value where $\Delta\omega = 0$

$$\frac{1}{2} R_e(\bar{E}' \cdot \bar{J}^*)_{peak} = -\frac{1}{2} \frac{1}{\nu} \frac{1}{\epsilon_o} |J|^2 \tag{54}$$

Numerically,

$$|J_{av}| = 1.5 \times 10^{-6} \frac{coul}{m^3} \times 3 \times 10^8 \frac{m}{sec} = 450 \text{ amp}/m^3 \tag{55}$$

and

$$\nu = 0.3 \times 10^6/\text{sec}$$

so that

$$\frac{1}{2}R_e(\bar{E}'.\bar{J}^*) = 4 \times 10^{10} \text{ watts/m}^3 \tag{56}$$

An upper limit to the total power yielded by the beam may be found by multiplying this figure by the volumn of the interaction region, 5×10^{-5} m^3, to give 2×10^6 watts. Because the plasma is so non-uniform in the interaction region the maximum value of the integrand may only be attained in a very small sub-region of the whole interaction region. For instance, the numerical value of the integrand may range between 4×10^4 and 4×10^{10} watts/m^3 (for Δf = 20 Mc and 0 Mc, respectively) within the interaction region, so the actual power extracted from the beam by the plasma would probably be closer to 2 watts than 2 Mw.

Calculation of the Energy Stored in the Electric Fields--Transient Behavior

Since the beam actually is fired in 0.1 μsec bursts, we must estimate how much energy is stored in the oscillating fields during the transient response to a burst of electrons.

The energy stored in the electric fields is given by the expression

$$\mathcal{E} = \int \frac{1}{2} \epsilon_o E^2 \, dv \tag{57}$$

Consider the transient behavior of the field during the 0.1 μsec that the beam is turned on. Unless the beam-plasma system is so close to resonance that collisions limit the fields, it will not matter if the collision frequency is assumed equal to zero. This is a convenience that allows the transient behavior to be found by applying a simple, tabulated Laplace transform to the steady state solution of equation 48.

To commence the Laplace transformation, write $s = i\omega$, and equation 48 becomes the expression

$$\text{Transform } E_z'(t') = \frac{s}{s^2 + \omega_p^2} \frac{v_b}{\epsilon_o} \text{ Transform}\left[\rho_s(r,t') \right] \tag{58}$$

where

$$t' = t - \frac{z}{v_b} \tag{59}$$

If

$$\rho_s(r,t') = \begin{cases} 0 & t' < 0 \\ \rho_o(r) \sin \omega' t & t' > 0 \end{cases} \tag{60}$$

Then

$$\text{Transform}\left[\rho_s(r,t') \right] = \rho_s(r) \frac{\omega'}{s^2 + \omega'^2} \tag{61}$$

and

$$\text{Transform } E_z'(t') = \frac{v_b}{\epsilon_o} \rho_o(r) \frac{s}{s^2 + \omega_p^2} \frac{\omega'}{s^2 + \omega'^2} \tag{62}$$

Finally,

$$E_z'(t') = 0 \qquad t' < 0$$

$$E_z'(t') = \frac{v_b}{\epsilon_o} \frac{\omega' \rho_o(r)}{\omega'^2 - \omega_p^2} \left[\cos \omega_p t' - \cos \omega' t'\right] \tag{64}$$

$$E_z'(t') = - \frac{v_b}{\epsilon_o \epsilon_r \omega'} \frac{\rho_o(r)}{2} \left[\sin\left(\frac{\omega' + \omega_p}{2}\right) t' . \sin \frac{\Delta\omega}{2} t'\right] \tag{65}$$

Besides oscillating at a frequency that is the average of f' and f, the electric field beats with a frequency $\Delta f/2$. If $\Delta f = 20$ Mcs on the axis of the vessel, then during a 0.1 μsec burst of electrons from the Linac the electric field there will beat once. However, the fields off the axis will be beating at slightly different frequencies, depending on the local value of ω_p. Furthermore, the intensity of the fields varies with position in the vessel, since E_z' depends on ρ/ϵ_r. That is, since the density of the Linac beam, ρ, falls off radially, the electric field is apt to be weak near the outer edge of the beam. And because ϵ_r depends on ω_p, it is a function of radial position.

When the 0.1 μsec burst of Linac electrons ends, the plasma electrons continue to oscillate for a while at the plasma frequency, so that the electric field does not disappear immediately. The oscillations are eventually damped out, either because of collisions between plasma electrons and gas molecules, or because of the decay of the plasma density.

The amplitude of the electric field is

$$(E_z')_{ampl} = \frac{v_b}{\epsilon_o \epsilon_r \omega} \frac{\rho_o(r)}{2} \tag{66}$$

Suppose $f = 20.400$ kMc and $f_p = 20.380$ kMc. Then $\epsilon_r \approx \frac{2\Delta f}{f} = 2 \times 10^{-3}$, which means that the field in plasma is 2000 times higher than the field in free space.

For the sixteenth harmonic $\rho_o = 1.5 \times 10^{-6}$ coulomb/m^3. Then the amplitude is

$$(E_z')_{ampl} = 8 \times 10^4 \text{ v/m.} \tag{67}$$

When the field strength according to equation 67, is 8×10^4 v/m the energy density is 0.03 joules/m^3. This energy density is not uniform throughout the beam-plasma interaction region, however, because the plasma density varies within the region. This variation of plasma density has two effects. Firstly, the electric field beats with different frequencies at different

distances from the axis. When the electric field on the axis is peaking, the field may be going through zero only a millimeter away. Secondly, the electric field is most intense where the plasma frequency is closest to the sixteenth beam harmonic. As we have already seen

$$n_o(r) = (n_o)_{axis} J_o(2.4 \frac{r}{a}) = (n_o)_{axis} J_o(r) \tag{68}$$

Near the axis,

$$n_o(r) = (n_o)_{axis} (1 - \frac{r^2}{4}) \tag{69}$$

$$\omega_p^2(r) = (\omega_p^2)_{axis} (1 - \frac{r^2}{4}) \tag{70}$$

$$\epsilon_r(r) = (\epsilon_r)_{axis} + \left(\frac{\omega_p^2}{\omega^2}\right)_{axis} \frac{r^2}{4} \tag{71}$$

$$= \left(\frac{2\Delta f}{f}\right)_{axis} + \frac{r^2}{4} \tag{72}$$

Suppose the plasma frequency on the axis were 20 Mcs greater than the sixteenth harmonic. Then, on the axis, $\epsilon_r = 2 \times 10^{-3}$. But, according to equation 72, the dielectric constant increases radially. This means that the electric field is most intense near the axis, and the energy density is greatest there. Only 0.27 cm away from the axis the dielectric coefficient increases to 2×10^{-2}, causing the peak energy density to decrease by 1/100.

On the other hand, suppose the plasma frequency on the axis were 20 Mcs smaller than the sixteenth harmonic. Then, on the axis, $\epsilon_r = -2 \times 10^{-3}$. The dielectric coefficient would increase to zero only 0.03 cm away from the axis, in the absence of collisions. The fields cannot actually go to infinity 0.03 cm from the axis because they are limited by a) collisional damping, b) the breakdown of linearity, c) lack of sufficient time for the fields to build up to a high value. These two cases lead to experimental approaches to resonance that can be achieved when a suitable time delay circuit is used.

A typical value of the stored energy density is the value when $f - f_p = 20$ Mc, i.e., 3×10^{-2} joules/m^3. The interaction volume is 5×10^{-5} m^3. The total energy stored in the interaction region is expected to be within several orders of magnitude of 3×10^{-2} joules/m^3 $\times$ 5×10^{-5} m^3 = 10^{-6} joules.

After the 0.1 μsec burst of electrons has been turned off, most of the stored energy will be dissipated in collisions between oscillating electrons and argon molecules, but some of it is expected to escape from the vessel. The energy will be dissipated in the time it takes the electrons to make several collisions, a time in the order of 10 μsec. The average rate of dissipation is then 0.1 watts. Only a small fraction of this need be radiated to

be detected by a sensitive receiver, provided it is not smeared out too thinly over the K-band spectrum.

It is expected that any radiation reaching a receiver outside the vessel will be spread over a broad frequency range. Suppose that radiation emerged from the vessel at one-millionth of the dissipation rate. Then the radiated power level might be 10^{-7} watts, based on the estimate above. Suppose that this is uniformly spread over the spectrum with a density of 10^{-7} watts/kMc because of the 1 kMc distribution of plasma frequencies in the interaction region.

The receiver can respond to radiation that is within two 8 Mcs passbands. (One band is 30 Mc above the intermediate frequency, and the other is 30 Mc below.) So, the level of radiated power that can be detected is 10^{-7} watts x 16 Mc/1000 Mc = 2 x 10^{-9} watts. Since the antenna (a K-band microwave horn) can intercept only 1/50 of the radiation emerging from the vessel, the detectable radiation is further reduced to 4 x 10^{-11} watts, which is somewhat larger than the sensitivity of the receiver (2.5 x 10^{-11} watts).

So, whether the radiation will be detected depends upon what fraction of the stored energy escapes from the vessel, the rate at which it escapes, and how thinly it is smeared over the spectrum.

APPARATUS

In addition to the linear accelerator, the apparatus consists of three major parts:

i. The experimental vessel, vacuum and gas system and plasma pulse generator.

ii. The microwave bridge and microwave receiver.

iii. Time delay circuitry and remote control circuitry.

The experimental vessel contains argon, which is ionized by a current spike from the d.c. pulser. The resulting plasma is allowed to decay and during its decay period it acts as a target for the Linac beam.

The microwave bridge and the microwave receiver serve different purposes, but their circuitry is interconnected in a combination bridge-receiver. The microwave bridge measures the electron density in the plasma vessel as a function of time. The receiver monitors the K-band microwave radiation which is expected to emerge from the vessel due to the passage of the Linac beam.

The time-delay and remote control circuitry are connected with the experimental vessel and the bridge-receiver. The time delay circuitry consists of a group of waveform and pulse generators. These establish a predetermined time relationship between pulsing the plasma and firing the Linac, and also trigger an oscilloscope display of the bridge diagnostic signal and the receiver gated output.

The remote control equipment is used because the level of radiation in the Linac target room is too high for personnel to be allowed in the room

whilst the accelerator is in operation. The remote control permits the receiver noise figure to be monitored. It also provides for the adjustment of the receiver frequency so that various portions of the microwave spectrum can be scanned. It also monitors the pressure of the argon in the vessel and the temperature of the vessel electrodes.

The Time-Delay Circuit

It is the object of the time-delay circuit to fire the Linac at a predetermined time in the decay of the plasma when the plasma frequency is close to the sixteenth harmonic frequency of the Linac beam. The frequency of the sixteenth harmonic is set at 20,800 kMc but the plasma frequency changes continually as the plasma decays.

Figure 6 is a timing diagram of the circuit. Waveform generator No. 1 furnishes signals to pulse generators No. 1 and No. 2 and establishes the basic repetition rate of the experimental cycle which is 100 msec. Pulse generator No. 1 furnishes a pulse of length 60 μsec to the plasma pulser, which ionizes the argon in the experimental vessel, creating an electron density greater than $4 \times 10^{12}/cm^3$. Pulse generator No. 2 triggers waveform generator No. 2 after a variable time delay. Waveform generator No. 2 supplies the receiver with a gate of duration 200 μsec and simultaneously actuates pulse generator No. 3. Pulse generator No. 3 inserts a small, variable time delay, then triggers the Linac.

The Experimental Vessel and the Plasma Pulser

The experimental vessel is shown in Figure 7. A-A' is the path followed by the Linac beam; the Kovar caps act as entrance and exit windows and also as electrodes, eliminating the need for internal electrodes. B-B' is the path of the microwave diagnostic signal. The cap thickness of 0.030 inches of the ferrous alloy, Kovar, causes approximately the same amount of scattering to the electron beam as the Linac exit window which is a thickness of 0.060 inches of aluminum. The total angular divergence of the beam is 10^{-3} radians (ref. 9).

The plasma pulser initiates the discharge with a 4000 V spike and then furnishes 15 A for 60 μsec. To determine the optimum argon pressure the output current waveform of the pulser was monitored with a current probe while the diagnostic bridge output was simultaneously observed. The appearance of these displays and the visual appearance of the discharge were studied as function of the gas pressure and the ballast resistance in series with the vessel. It was determined that when the argon pressure was between 0.1 and 0.15 torr and the ballast resistance was between 20 and 75 ohms:

a. There was a uniform brightness between A and A', partly extending into the cross between B and B'.

b. The initial plasma density was greater than $4 \times 10^{12}/cm^3$, as indicated by the microwave bridge.

c. The pulser current and the microwave bridge display repeated uniformly.

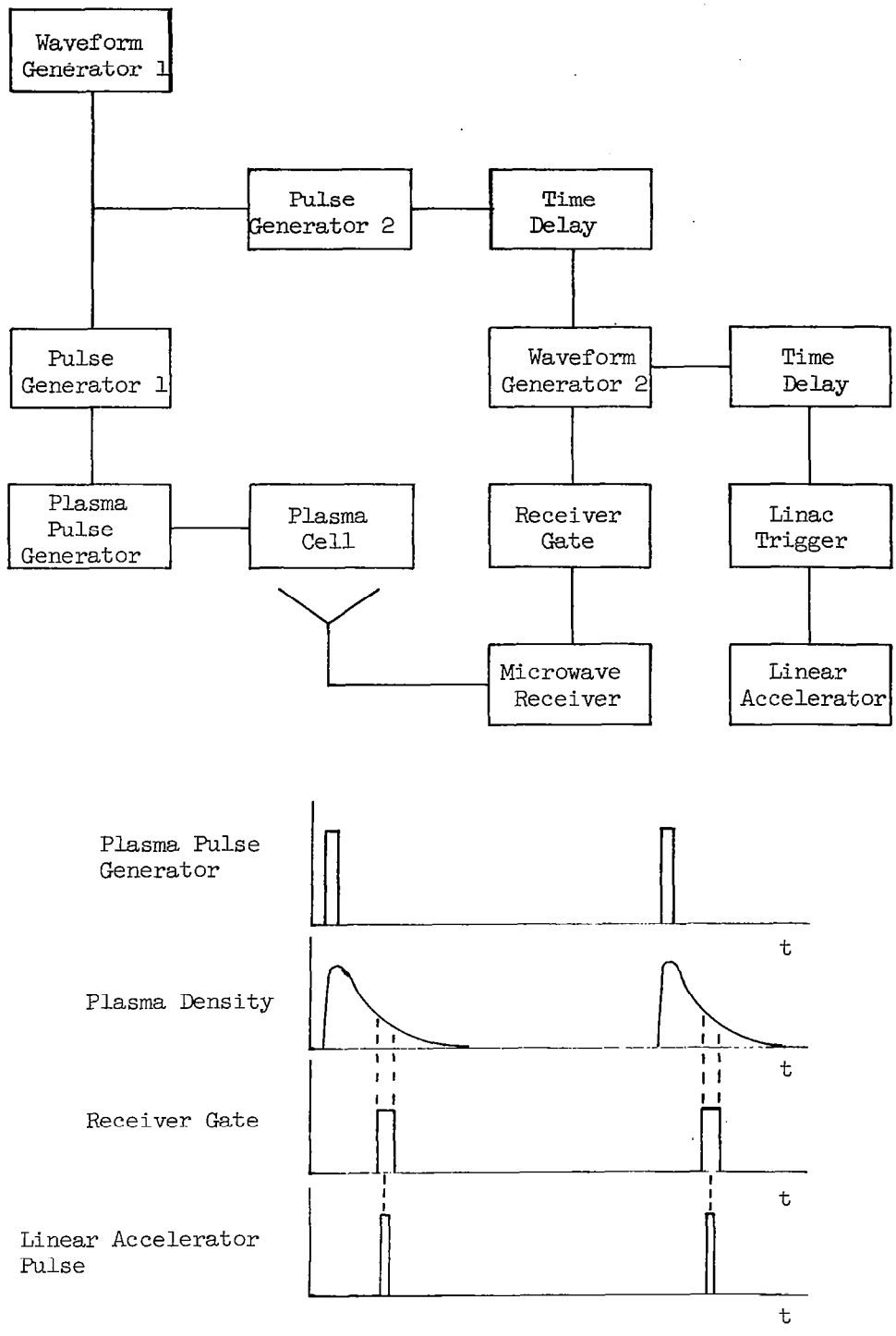

Timing diagram for the experiment

Figure 6

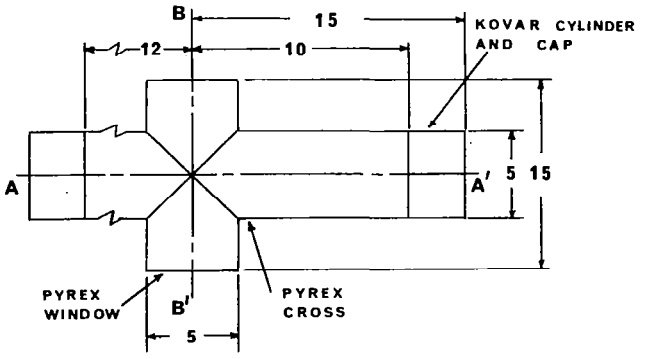

Figure 7. The experimental vessel, showing the path followed by the Linac Beam (A-A') and the path of the microwave diagnostic signal (B-B'). Dimensions are in cm.

In the final experimentation an argon pressure of 0.115 torr was employed. A ballast resistor of 25 ohms was chosen and coaxial cable was used for all leads to minimize spurious radiation due to pulsing.

The Combination Receiver and Bridge

Figure 8 depicts the microwave components of the bridge-receiver. The flow of microwave signal in the bridge-receiver depends upon the position of the microwave switch, which can be remotely actuated from the control room. The receiver noise figure may be observed at any time during the experiment by actuating the microwave switch and it affords a convenient check against deterioration of the receiver performance.

Receiver sensitivity - The receiver output noise power before detection N_o is given by the expression

$$N_o = k\, T_1\, B\, F\, G \tag{73}$$

where T_1 is the antenna temperature, 300^oK;

B is the receiver bandwidth, 8 Mc

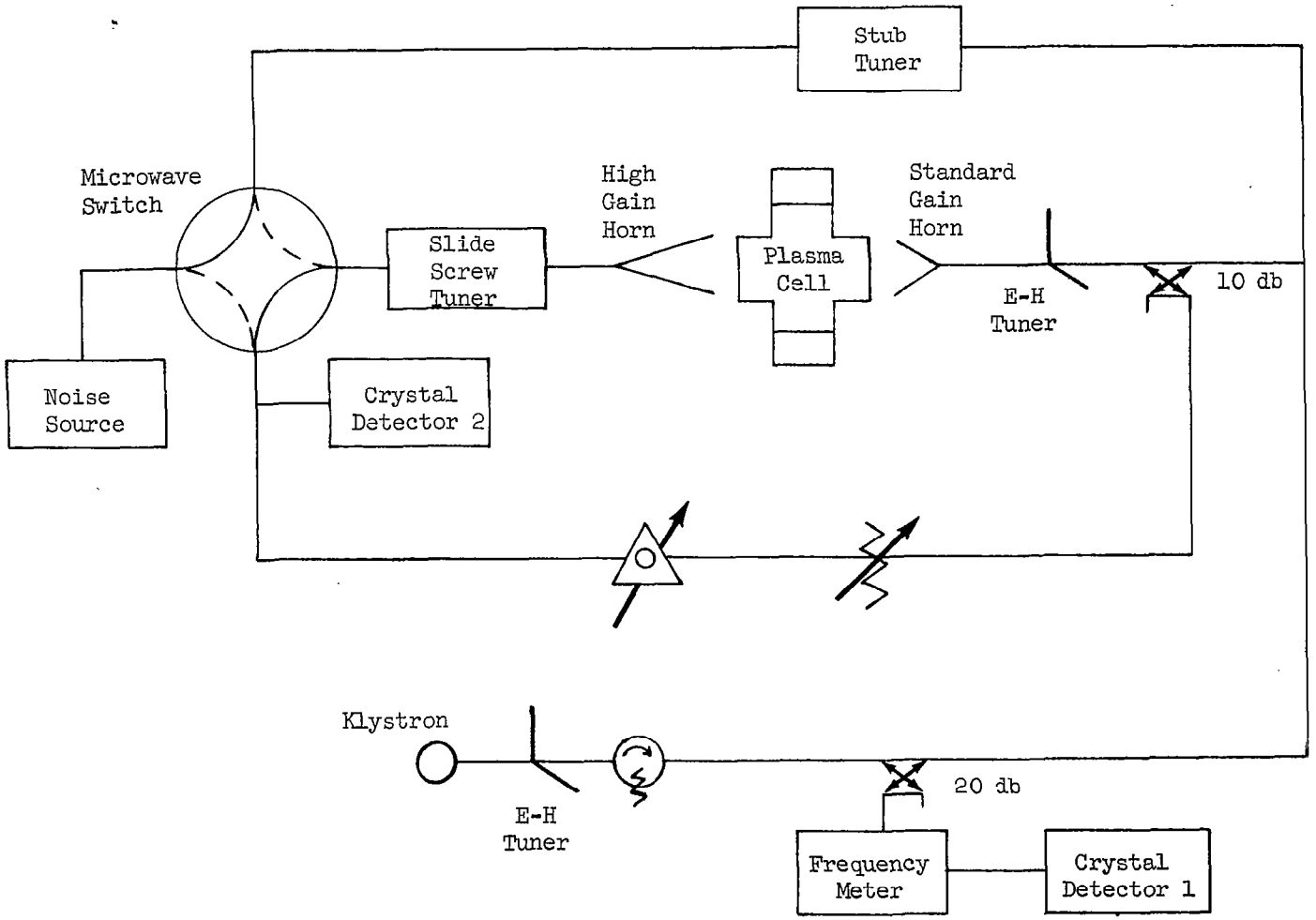

Figure 8. Microwave Bridge - Receiver Circuit.

G is the receiver gain

F is the receiver noise figure.

The receiver signal output power is

$$S_o = S_i\, G \tag{74}$$

where S_i is the input signal power.

Measurement of the receiver noise figure is accomplished by connecting the pulsed standard noise source to the balanced crystal mixer. The noise source is a section of waveguide that contains a gas discharge which is backed up by a matched termination. The noise source simulates an antenna temperature of $T_1 = 300^{\circ}K$ when the discharge is off and an antenna temperature of $T_2 = 9600^{\circ}K$ when the discharge is on.

When the source is off, receiver output power is

$$N_1 = k\, T_1\, B\, F\, G \tag{75}$$

But when the source is on, receiver output power is

$$N_2 = k\, T_1\, B\, (F-1)\, G + k\, T_2\, B\, G \tag{76}$$

When sufficient attenuation, α, is inserted between the pre-amplifier and the amplifier to equalize these two powers, then

$$k\, T_1\, B\, (f-1)\, G + k\, T_2\, B\, G = \alpha\, k\, T_1\, B\, F\, G \tag{77}$$

so that

$$F = \frac{(T_2/T_1) - 1}{\alpha - 1} \tag{78}$$

Throughout the experiment the noise figure was between 12 and 13 db.

From equations 73 and 74 we obtain

$$\frac{S_o}{N_o} = \frac{S_i}{k\, T_1\, B\, F} = \frac{S_i}{5 \times 10^{-13} \text{ watts}} \tag{79}$$

When the input power is greater than 5×10^{-13} watts the output signal-to-noise ratio is greater than unity and the signal can be discerned against the noise background. For this reason, 5×10^{-13} watts is referred to as the sensitivity of the receiver. The second detector of the amplifier is followed by a 200 kcs filter. This has the effect of extending a 0.1 μsec signal to 5 μsec, but it also reduces the amplitude of the signal by a factor of $0.1/5 = 1/50$. This reduces the effective sensitivity to 2.5×10^{-11} watts.

In order to examine the microwave spectrum in the neighborhood of the sixteenth harmonic of the Linac beam it is necessary to make several changes in the local oscillator frequency of the receiver. Small changes can be accomplished by varying the reflector voltage of the local oscillator klystron. Changes of more than 20 Mc can be made by a mechanical adjustment of the size of the klystron cavity. For example, suppose that the local oscillator frequency has been set to 20,770 Mc. Then the frequency may be changed up to 20 Mc in either direction by varying the reflector voltage. The device shown in Figure 9 is provided for this purpose. It can be adjusted in the control room. It is used to make local oscillator changes in steps of $\pm$ 5 Mc. When

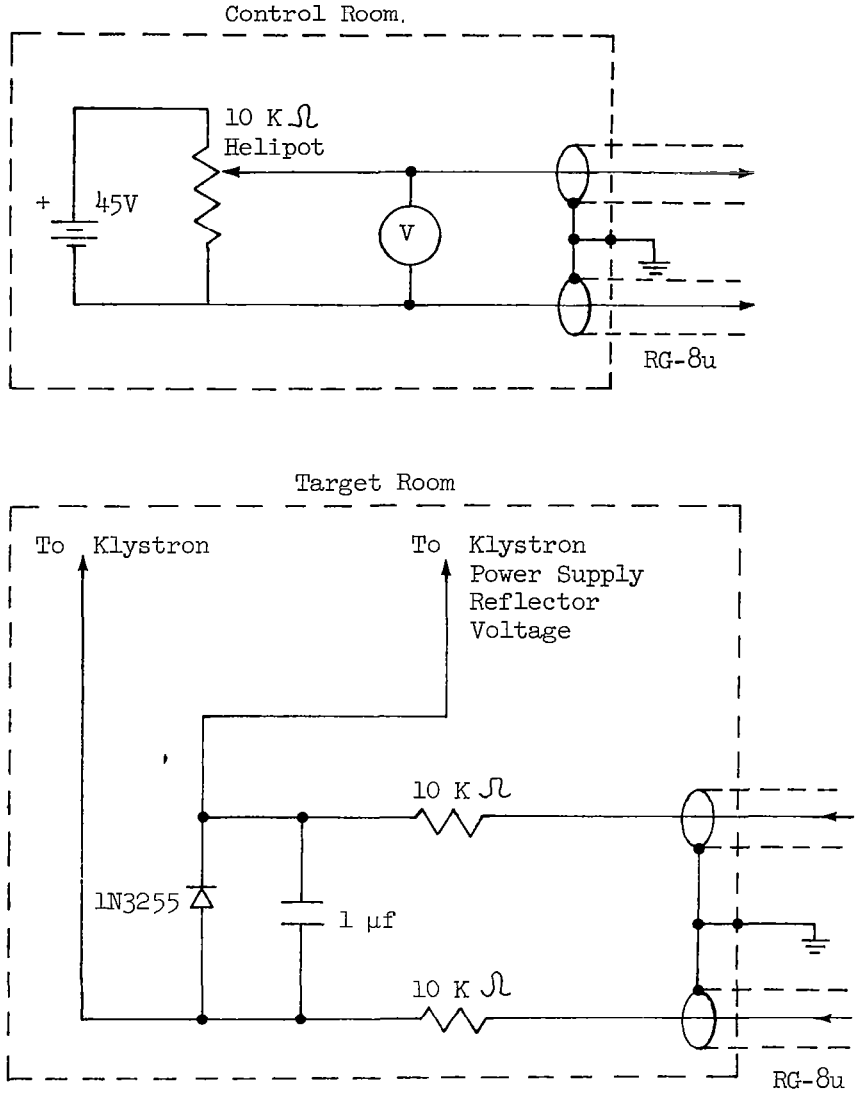

Scheme for changing the local oscillator frequency by changing the klystron reflector voltage remotely from the control room.

Figure 9

a frequency change of greater than 20 Mcs is desired it is necessary to enter the Linac target room and adjust the klystron cavity. Then the entire bridge-receiver must be retuned, including the antenna tuners and the balanced crystal mixer.

The precision of the frequency meter used to measure and set the receiver local oscillator frequency is 20 Mc, as stated by the manufacturer and confirmed by calibration against a high harmonic crystal. The frequency meter is a tunable microwave cavity. The fundamental frequency of the Linac is also measured with a tunable cavity. According to the manufacturer of the Linac (private communication, 1963) the cavity is calibrated against a known frequency source whose absolute accuracy is 1 part in 10^6. But the basic accuracy of the unit is determined by the accuracy of resetting the tuning dial, which is about 25 kcs. Thus the frequency of the 16th harmonic is known within 400 kcs. For instance, the change of phase of the diagnostic signal in traversing a path length, D, of un-ionized gas is

$$(\Delta\phi)_F = 2\pi \frac{D}{\lambda} \tag{80}$$

where λ is the free space wavelength. The change of phase in traversing the same path length filled with plasma

$$(\Delta\phi)_p = 2\pi \frac{D}{\lambda} \langle \epsilon_r^{1/2} \rangle \tag{81}$$

Here $\langle \epsilon_r^{1/2} \rangle$ is the average index of refraction. The net change of phase due to the presence of the plasma is

$$(\Delta\phi)_{net} = \frac{2\pi D}{\lambda} \left[1 - \langle \epsilon_r^{1/2} \rangle \right] \tag{82}$$

When the net phase shift is 180°, 540°, 900°, etc., the bridge is completely unbalanced. When the phase shift is 360°, 720°, 1080°, etc., the bridge is rebalanced. When the plasma frequency exceeds the diagnostic frequency the microwave signal cannot propagate through the plasma and the bridge is unbalanced. The signal cannot traverse the plasma because

$$\epsilon_r^{1/2} = (1 - \omega_p^2/\omega^2)^{1/2} \tag{83}$$

When $\omega_p > \omega$ the index is imaginary; instead of propagating the microwaves are evanescent.

The signal from crystal detector No. 2 is displayed on an oscilloscope and Figure 10 is a drawing of the pattern of "fringes" observed furing the decay of the plasma. Point A is the last fringe of the plasma build-up. Region B is the interval during which the plasma density is so high that the microwaves cannot propagate through the plasma. Points C, D, E, F, and G represent phase shifts of 900°, 720°, 540°, 360°, 180° and 0°.

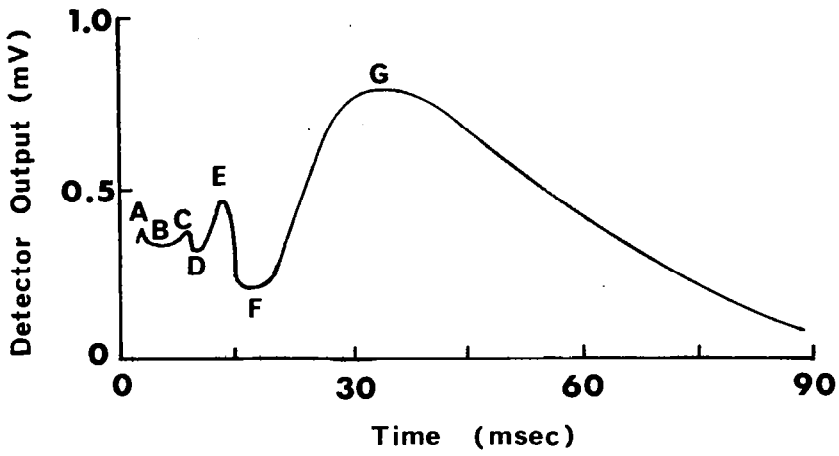

Pattern of fringes observed on crystal detector No. 2 during plasma decay. For explanation of lettered curve see the text.

Figure 10

PROCEDURE AND RESULTS

The point at which the beam emerged from the Linac's exit window was located by placing a sheet of transparent plastic in the beam and observing where it became darkened. The plasma cell was then placed in the beam and a lead brick was placed behind the vessel to catch the beam and give a relative measure of beam current. (The possible errors in measuring current with a beam catcher are explained by Choderow, (ref. 12)). The microwave bridge was put in place and the crystal mixer, the crystal detectors, and the i.f. pre-amplifiers, the noise figure meter, and the klystron power supply were placed in the target room where they would not receive direct irradiation from the Linac.

The receiver local oscillator frequency was set to 20.770 kMc, which centered the receiving bands at 20.740 kMc. (Figure 11).

A search for radiation was initiated at a beam current of 0.010 amp. The time delay controlling the receiver gate was varied over its full range at the same time sweeping the Linac beam through the entire afterglow duration of the discharge. When no radiation was detected the search was repeated at values of local oscillator frequency between 20.750 and 20.790 kMc. These frequencies were attained by varying the reflector voltage. Again, no signal was detected. Since the vessel had shown no signs of overheating, it was decided to increase the peak beam current to 0.300 amp. Repeating the previous search at the higher current level no radiation was detected. There then followed a series of searches in which the local oscillator frequency was adjusted over a wide interval by manually adjusting the klystron cavity size. This permitted covering the entire frequency range between 20.670 kMc and 20.870 kMc as is depicted in Figure 11. No radiation was detected. Furthermore there was no evidence from the diagnostic display on the oscilloscope that the plasma density was affected by the beam.

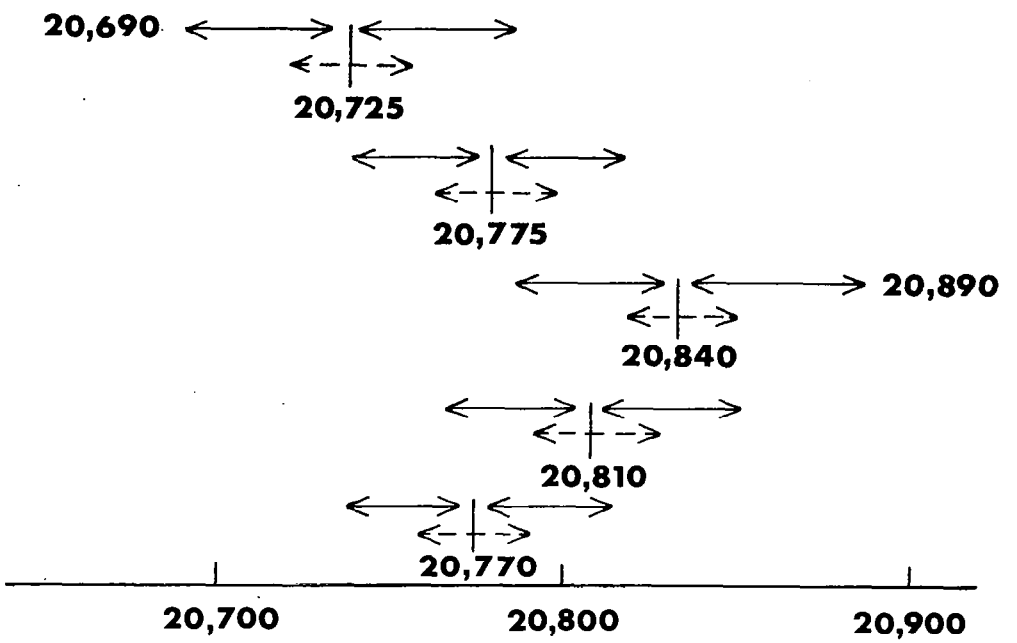

Frequency diagram showing five settings of Local oscillator frequency (vertical lines), the range of electrical tuning (horizontal dotted lines) and the corresponding change in upper and lower receiver passbands (horizontal solid lines)

Figure 11

CONCLUSIONS

The passage of an electron beam through a gas discharge may initiate plasma oscillations that can be detected with probes, or by radiation outside the discharge vessel. According to one school of thought, the oscillations are due to the way the discharge as a whole, especially the electrode sheath, modulates and manipulates the electron beam. The Looney-Brown experiment (ref. 3) provides evidence for this viewpoint, at least for a specially contrived vessel. On the other hand, the oscillations can be ascribed simply to the interaction between a modulated electron beam and the plasma electrons acting independently of electrode sheaths. The plasma oscillation experiments that have been performed since the Looney-Brown experiment have shed no light on whether sheaths are necessary to cause oscillations. Furthermore, these experiments have been marred by the use of probes to detect the electron oscillations in the beam-plasma interaction region. It must always be borne in mind that probes perturb the plasma, perhaps even causing spurious oscillations.

It was the object of this experiment to fire the Linac beam through a decaying plasma and search for radiation outside the vessel due to interaction of an harmonic of the beam with the plasma. It was expected that the Linac beam would have a high harmonic content and an analysis of representative energy spectrum measurements of the beam in terms of the accelerator operation confirms that the sixteenth harmonic content is substantial. That

is, a peak beam current of 0.3 amp. contains a 20.8 kMc Fourier component equivalent to a pure rf current of 0.1 amp. This frequency is close to the plasma frequency so that a resonance effect is expected to give rise to electron oscillations.

The receiving antenna had an effective area of 75 cm^2. It was located 25 cm from the vessel, where it intercepted 1/50 of the power radiated from the vessel. The receiver was expected to respond to radiation at a level higher than 2.5×10^{-11} watts. It can therefore be concluded that the power emitted from the vessel is less than 1.25×10^{-9} watts, or 0.4×10^{-10} watts per cm of path traversed by the beam. Thus there is weak coupling between the plasma oscillations stimulated by the beam and the radiation field.

APPENDIX

HARMONIC ANALYSIS OF THE LINAC BEAM

Charge Density and Phase Distribution

Bunches of electrons emerge from the Linac with a frequency $\omega_L = 2\pi \times 1.3 \times 10^9$/sec. Since their energy is about 40 Mev their speed, v_b, is very close to 3×10^{10} cm/sec. Suppose the electrons move in the z-direction; then the charge density along their path is a function of $(z - v_b t)$. Figure 12 depicts the charge density plotted against three different abscissas.

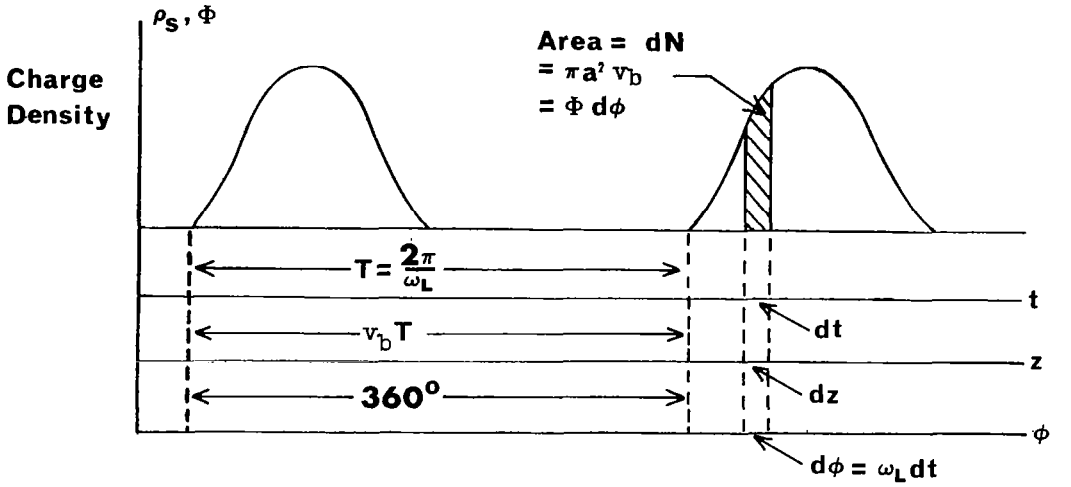

Charge density in Linac beam measured with respect to time, distance along the beam, and phase of the electron bunches.

Figure 12

Using the first abscissa gives a plot of charge density vs. time at some fixed value of z. Using the second gives a plot of charge density vs. position at some instant. Using the third gives a plot of charge density vs. phase. The spacing between bunches is 0.77×10^{-9} sec, 23.0 cm or 360°, depending on which scale is used.

The number of electrons that pass an observer in the time dt is

$$dN = \rho(t)\, \pi a^2\, v_b dt \qquad \text{(I-1)}$$

This same number of electrons is contained in a phase interval $d\phi = \omega_L\, dt$, so

$$dN = \rho\, \pi a^2 \frac{v_b}{\omega_L} dt = \Phi(\phi)\, d\phi \qquad \text{(I-2)}$$

It is possible to think of the electron density as being measured by ρ, which is a function of $(z - v_b t)$ or as being measured by Φ, which is a

function of phase. From I-2

$$\Phi(\phi) = \frac{\pi a^2 \mu}{\omega_L} \rho(z - v_b t) \tag{I-3}$$

Fourier Analysis of the Charge Density

Since the density of electrons from the Linac is periodic, it is convenient to decompose the density into its Fourier components.

$$\rho(z - v_b t) = \frac{q}{\pi a^2} \sum_{N=-\infty}^{\infty} \eta_N e^{i \frac{\omega_N}{}(z - v_b t)} \tag{I-4}$$

where $\omega_N = N \omega_L$. (Since πa^2 is the cross-sectional area of a bunch, and $v_b t$ is the distance between bunches, $q/\pi a^2 v_b t$ is the average charge density per cycle.)

The expression for η_N is derived in the following way: If

$$\rho\left(t - \frac{z}{v_b}\right) = \sum_{N=-\infty}^{\infty} \hat{\rho}(\omega_N, z)\, e^{-i\omega_N t} \tag{I-5}$$

then

$$\rho(\omega_N, t) = \frac{1}{T} \int_{t=o}^{t=T} \rho\left(t - \frac{z}{v_b}\right) e^{i\omega_N t}\, dt \tag{I-6}$$

$$= \frac{1}{T} \int_{t-\frac{z}{v_b} = o}^{t-\frac{z}{v_b} = T} \rho\left(t - \frac{z}{v_b}\right) e^{i\omega_N t}\, dt \tag{I-7}$$

$$= e^{i \frac{\omega_N z}{v_b}} \frac{1}{T} C_N \tag{I-8}$$

where

$$C_N = \int_{t'=o}^{t'=T} \rho(t') e^{i\omega_N t'}\, dt' \tag{I-9}$$

The total charge in a bunch, q, is

$$q = \pi a^2 v_b \int_{t=o}^{t=T} \rho\left(t - \frac{z}{v_b}\right) dt \tag{I-10}$$

$$= \pi a^2 v_b 2\, C_o \tag{I-11}$$

where

$$C_o = \frac{1}{2} \int_{t'=o}^{t'=T} \rho\,(t')\,dt' \qquad \text{(I-12)}$$

From equations I-8 and I-12

$$\hat{\rho}\,(\omega_N,\ z) = e^{i\frac{\omega_N z}{v_b}} \frac{q}{\pi a^2 v_b T} \frac{C_N}{2C_o} \qquad \text{(I-13)}$$

Substituting in equation I-5

$$\rho(t - \tfrac{z}{v_b}) = \sum_{N=-\infty}^{\infty} \frac{q}{\pi a^2 v_b t} \frac{C_N}{2C_o}\ e^{i\frac{\omega_N}{v_b}(z - v_b t)} \qquad \text{(I-14)}$$

Then, by comparison with equation I-4

$$\eta_N = \frac{C_N}{2C_o} \qquad \text{(I-15)}$$

It is the purpose of this Appendix to evaluate η_N for the first 32 harmonics of the Linac beam.

The Acceleration of Electrons

Acceleration occurs in a series of nine identical microwave cavities, which are excited by high power klystrons. Each cavity is connected to its neighbor by an opening in its end walls, so electrons may move from one cavity to another. Because the nine cavities comprise a periodic structure, the longitudinal electric field established between the ends of the accelerator may be resolved into a Fourier sum of traveling waves propagating up and down the accelerator, with phase velocities greater and smaller than the speed of light. If the phase relationship between cavities is properly adjusted, a wave will propagate down the accelerator with the speed of light. This wave is known as the synchronous wave because electrons traveling down the accelerator with speeds close to 3×10^{10} cm/sec maintain an almost constant phase relationship with the wave.

The electrons are injected with an energy of 100 kev. They are compressed into bunches by the klystron-like action of a buncher cavity. Then they enter the first rf cavity, in which their energy is increased to several Mev. Upon leaving the first cavity the electrons are traveling at very close to the speed of light and are almost synchronous with the accelerating wave. The extent of "slippage" between the electrons and the wave can be estimated as follows:

When the electron and the synchronous wave travel a short distance, δL, the electron slips behind in phase by

$$\delta\phi = -\omega \delta L\left(\frac{1}{\nu_{EL}} - \frac{1}{\nu_{wave}}\right) \qquad \text{(I-16)}$$

$$= -\omega \delta L\left(\frac{1}{\beta c} - \frac{1}{c}\right) \qquad \text{(I-17)}$$

The energy of the electron is given by

$$W = \frac{m_o c^2}{(1-\beta^2)^{1/2}} \qquad \text{(I-18)}$$

where m_o = the rest mass of the electron, and since $\beta \approx 1$

$$1 - \beta \approx -\frac{1}{2}\left[\frac{m_o c^2}{W}\right]^2 \qquad \text{(I-19)}$$

Then

$$\delta\phi \simeq -\frac{\omega}{c}\ \delta L(1-\beta)$$

$$= \frac{\omega}{2c}\ \delta L\left(\frac{m_o c^2}{W}\right)$$

Assume the electron energy increases linearly with distance, so that

$$W_f = W_i + \gamma L \qquad \text{(I-20)}$$

(For the R.P.I. Linac a typical value of γ is 5 Mev/meter.) In traversing a distance L and increasing its energy from W_i to W_f, the electron slips behind in phase by

$$\Delta\phi = -\frac{\omega}{2c}(m_o c^2)^2 \int_{L'=0}^{L'=L} \frac{\gamma L'}{(\gamma L' + W_i)^2}\, dL' \qquad \text{(I-21)}$$

$$\Delta\phi = -\frac{\omega}{2c}\ \frac{(m_o c^2)^2}{\gamma}\left(\frac{1}{W_i} - \frac{1}{W_f}\right) \qquad \text{(I-22)}$$

$$= -\frac{\omega}{c}\,(-8.2)\left(\frac{1}{W_i} - \frac{1}{W_f}\right) \text{ degrees/Mev} \qquad \text{(I-23)}$$

From equation I-23 the slippage can be calculated. The result is shown in table I-1. Thus, there is very slight slippage when $W > 3$ Mev.

Figure 13 depicts the longitudinal component of the electric force on an electron as a function of its phase with respect to the synchronous wave. The figure also depicts the electron density of a typical bunch. It has just been shown that if the energy of the electrons in the bunch is greater than about 3 Mev the bunch maintains almost a constant phase relationship with the wave.

Table I-1

From	To	Slippage is
3 Mev	5 Mev	1.07°
5	10	0.82°
10	15	0.28°
15	20	0.13°
20	25	0.08°

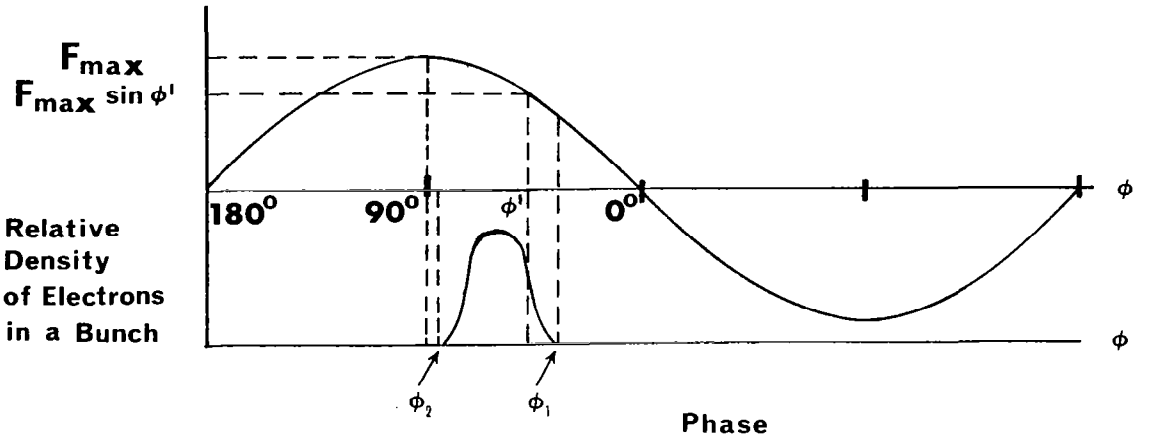

Longitudinal Electric field force on an electron in a bunch and relative density of a bunch as a function of its phase with respect to the phase of the synchronous wave.

Figure 13

The electrons nearest the crest of the wave ($\phi = \phi_2$, in Figure 13) feel the strongest electric force. Electrons farther from the crest feel weaker forces.

$$F \sim \sin \phi \tag{I-24}$$

The total energy of an electron that emerges from the Linac is the sum of the energy which it acquired before achieving synchronization (roughly 3 Mev) plus the integral of force x distance in the remainder of the accelerator.

$$W = 3 + \int F \, dl \tag{I-25}$$

$$= 3 + \sin \phi \int F_{max} \, dl \tag{I-26}$$

Since the electrons are "strung out" in phase, all the members of a bunch do not acquire the same energy in traversing the Linac. For instance, the foremost electrons in a bunch ($\phi = \phi_1$) acquire the energy

$$W_1 = 3 + \sin \phi_1 \int F_{max}\, dl \qquad \text{(I-27)}$$

the rearmost electrons acquire the energy

$$W_2 = 3 + \sin \phi_2 \int F_{max}\, dl \qquad \text{(I-28)}$$

and intermediate electrons acquire the energy

$$W = 3 + \sin \phi \int F_{max}\, dl \qquad \text{(I-29)}$$

Thus, the rearmost electron acquires the most energy in the Linac. This is the principal cause of the relatively broad spectrum of energies exhibited by electrons emerging from a linear accelerator.

The Linac Energy Spectrum

The energy spectrum of electrons emerging from the Linac is measured with a magnetic analyser. Electrons are deflected through an arc of radius r by a magnetic field of strength H.

$$r = \frac{W}{C}\ \frac{1}{eH} \qquad \text{(I-28)}$$

A Faraday cup is located behind a slit that admits all electrons that have been deflected through arcs of radius between r and $r + dr$. Thus the slit admits electrons with energies between W and $W + dW$, where

$$dW = C\ e\ H\ dr \qquad \text{(I-29)}$$

From equations I-28 and I-29 $\frac{dW}{W} \sim \frac{dr}{r}$. Since r and dr are fixed by the geometry of the analyser

$$dW \sim W \qquad \text{(I-30)}$$

Figure 14 depicts the energy spectrum of a (hypothetical) group of electrons. The number of electrons with energies between W_1 and $W_1 + dW_1$ is $dN_1 = C(W_1)\, dW_1$, which is the shaded area under the curve. Similarly, the number of electrons with energies between W_2 and $W_2 + dW_2$ is $dN_2 = C(W_2)\, dW_2$. Suppose $C(W_1) = C(W_2)$. According to equation I-30 the spectrum analyser takes a broader "slice" of the energy spectrum at the higher energy, W_2, then at the lower energy, W_1. Hence,

$$\frac{dN_1}{dN_2} = \frac{C(W_1)\, dW_1}{C(W_2)\, dW_2} = \frac{dW_1}{dW_2} = \frac{W_1}{W_2} < 1 \qquad \text{(I-31)}$$

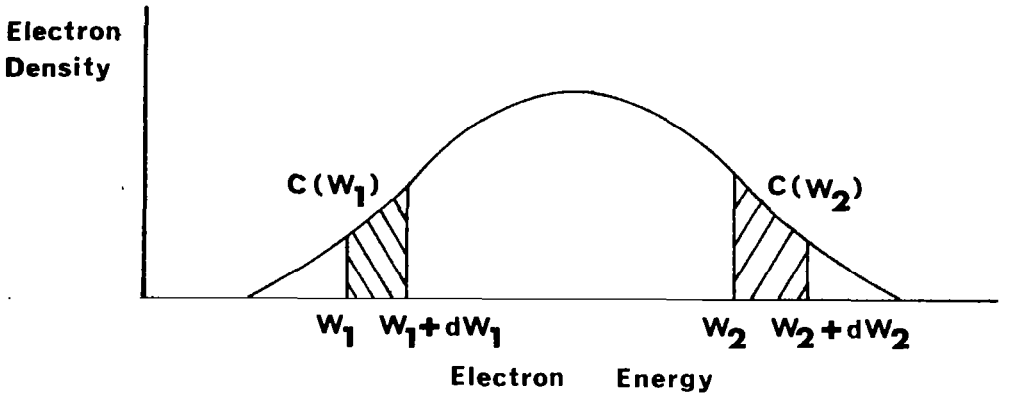

Theoretical energy distribution of an
electron bunch emerging from the Linac.

Figure 14

Although the energy spectrum has the same height at W_1 as at W_2, the spectrum analyser collects more electrons at the higher energy. This means that the graph of collected current vs magnetic field strength is not the energy spectrum, but a distortion of the energy spectrum. The graph is often referred to as the undivided energy spectrum to distinguish it from the true energy spectrum.

Thirteen measurements of the undivided energy spectrum of the R.P.I. Linac were made by Dr. Kiwalski, and four sets of collector current vs. analyser magnet current readings are shown in Figure 15. The curves shown are the first, second, third and ninth sets and the other nine sets closely resemble the ones shown in Figure 14 both in shape and in width.

The true energy spectrum, (C(W)), is calculated from the undivided energy spectrum in the following way:

i. The current in the analyser magnet, I_M, is a measure of the electron energy. Multiply it by 23.8 Mev/A to obtain the energy.

$$W = 23.8\ I_M \tag{I-32}$$

ii. The current collected in the Faraday cup, i_c, is the height of the undivided spectrum. Divide it by W to obtain the height of the true spectrum.

$$C(W) \sim \frac{i_c}{W} \sim \frac{i_c}{I_M} \tag{I-33}$$

Analyzing the Undivided Energy Spectrum

It was shown in section 3 that the energy of an electron depends upon its phase relative to the synchronous wave. The electrons nearest the peak of the wave acquire the greatest energy, W_2, in the Linac, while electrons

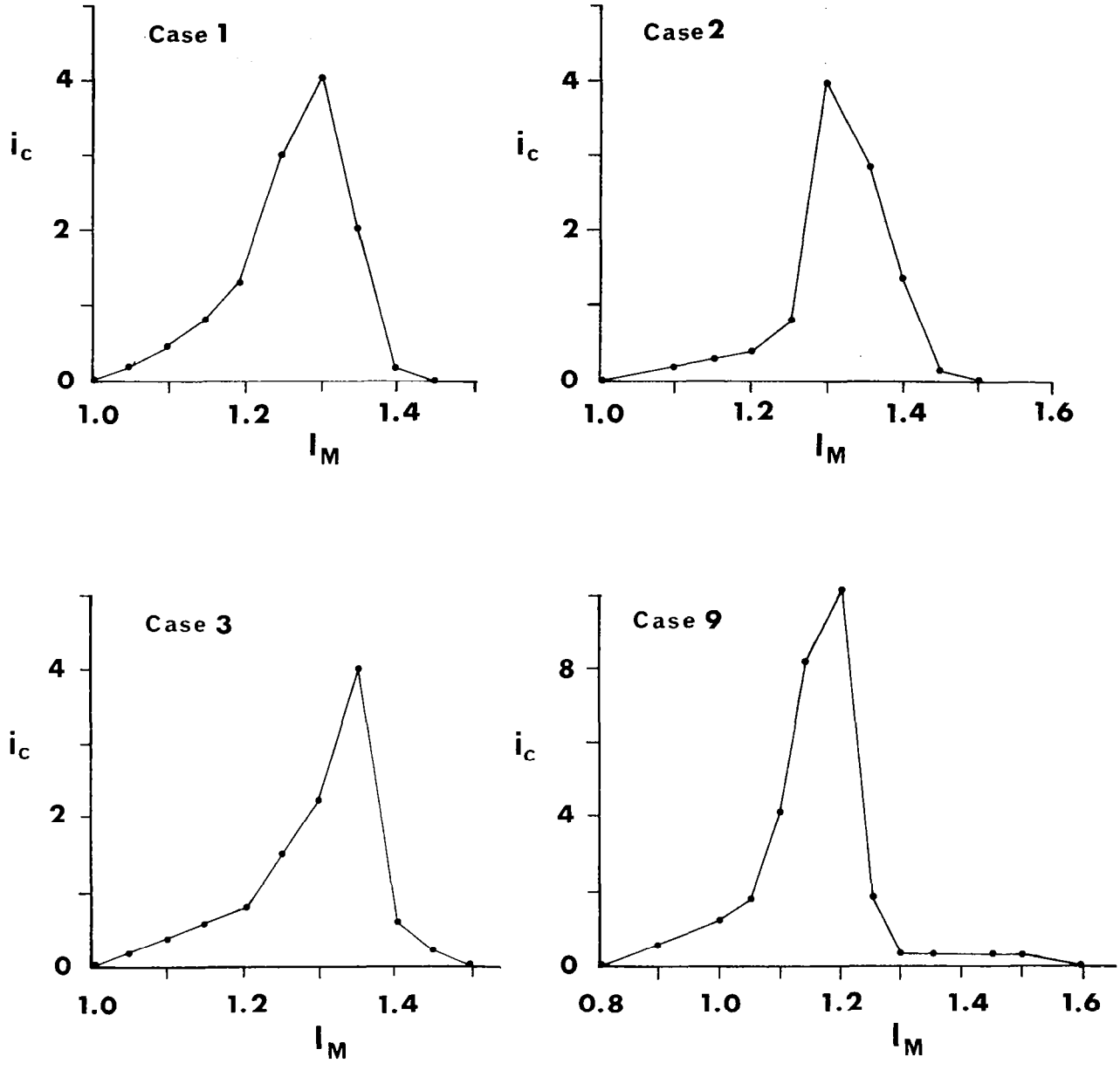

Collector Current vs. Analyzer Magnet Current

Distorted or undivided energy spectrum of Linac beam as recorded in the Linac log book.

Figure 15

farther from the peak ($\phi < \phi_2$) acquire lesser energies ($W < W_2$). According to equation I-28 and I-29,

$$\sin \phi = \frac{W-3}{W_2-3} \sin \phi_2 \qquad \text{(I-34)}$$

If $\phi_2 = 90^\circ$ equation I-34 can be rewritten

$$\sin \phi = \frac{W-3}{W_2-3} \qquad \text{(I-35)}$$

Then equation I-35 may be used to establish a relationship between the electron energies and their position with respect to the rf wave. For instance, take case No. 1 of Figure 15. The highest energy measured is 1.45 A x 23.8 Mev/A = 34.5 Mev and the energy of the peak is 1.30 A x 23.8 Mev/A = 31.0 Mev. So according to equation I-35, the 31.0 Mev electrons had a phase given by

$$\sin \phi = \frac{28.0}{31.5}, \phi = 67^\circ$$

The number of electrons in the energy range of width dW is $dN = C(W)\, dW$. The same electrons occupy a phase range of width $d\phi$. (In fact, the spread in energies is due to the spread in phase.) Then

$$dN = C(W)\, dW = \Phi(\phi)\, d\phi \qquad \text{(I-36)}$$

or

$$(\phi) = C(W) \frac{dW}{d\phi} \qquad \text{(I-37)}$$

Now, from the derivative of equation I-35

$$\frac{dW}{d\phi} = \cos \phi (W_2 - 3) \qquad \text{(I-38)}$$

So

$$(\phi) = C(W) \cos \phi \qquad \text{(I-39)}$$

To calculate the phase distribution from the true energy spectrum:

i. For every value of W, calculate ϕ from

$$\sin \phi = \frac{W-3}{W_2-3} \qquad \text{(I-40)}$$

ii. For every value of C(W) calculate $\Phi(\phi)$ from

$$(\phi) = C(W) \cos \phi \qquad \text{(I-41)}$$

The graph of ϕ, Φ gives the phase distribution of electrons in a bunch. Thus, working first with the undivided spectrum, and then the true spectrum, it is possible to calculate the shape of a bunch of electrons emerging from the Linac.

The relations between the abscissas and the ordinates of the three types of spectra are shown in Table I-2.

Table I-2

Undivided Spectrum	True Energy Spectrum	Phase Distributions
I_M	$W = 23.8\ I_M$	$\phi = \sin^{-1}\left[\frac{W-3}{W_2-3}\right]$
i_c	$C(W) = \frac{i_c}{I_M}$	$\Phi = C(W)\cos\phi$ $= \frac{i_c}{I_M}\cos\phi$

The analyzer magnet current was read on a 0-3 A meter, and measurements of the current are subject to errors of 0.005 A, a limit which is set by the observer's ability to interpolate between scale readings. The collected current was measured with a multi-scale micro-micro-ammeter. The error is larger for this current, because any one of the scales may be in error by 5% of the full scale value. The following rules can be applied:

a. For current between 3 μA and 10 μA, the error is 0.5 μA. (5% of a full scale.)

b. For current between 1 μA and 3 μA, error is 0.17 μA. (5% of full scale.)

c. For currents below 1 μA, error is 0.05 μA. (Error in plotting data into log book and reading it out.)

The errors in the measured currents result in errors in the abscissa and the ordinate of the phase distribution. The error in the abscissa is calculated from

$$\delta\phi = \frac{23.8}{W_2-3}\ \frac{1}{\cos\phi}\ \delta I_M \tag{I-42}$$

where δI_M is the error in the magnet current. The error in the ordinate is given by

$$\frac{\delta\Phi}{\Phi} = \frac{\delta i_c}{i_c} + \tan\phi\ d\phi + \frac{\delta W}{W} \tag{I-43}$$

But it turns out that, as a consequence of the fact that the relative error in i_c is much larger than the relative error in I_M

$$\frac{\delta i_c}{i_c}\tan\phi\ d\phi + \frac{\delta W}{W} \tag{I-44}$$

Then

$$\frac{\delta\Phi}{\Phi} = \frac{\delta i_c}{i_c} \tag{I-45}$$

The computed values for cases No. 1, No. 2, No. 3 and No. 9 are shown in Tables I-3 to I-6. The columns are computed in the following fashion:

(a) is the measured analyzer magnet current, I_M, in amperes.

(b) is the corresponding electron energy, 23.8 Mev x I_M.

(c) is the value of (b) minus the largest value of W.

(d) is $\sin \phi = (W-3)/(W_2-3)$

(e) is ϕ

(f) is $\cos \phi$

(g) is the error in ϕ

$$\delta\phi = \frac{23.8}{W_2-3} \times \frac{I}{\cos\phi} \times \frac{360^\circ}{2\pi}$$

(h) is the measured value of collected current, i_c.

(i) is the error in collected current, assigned according to the rules above.

(j) is $C(W) = i_c/W$

(k) is $\Phi(\phi) = C(W) \cos \phi$

(l) is $\delta i_c/i_c$

(m) is $\delta \Phi = \Phi \delta i_c/i_c$

The phase distributions are plotted in Figure 16.

Fourier Analysis of the Phase Distribution

The phase distribution curves of Figures 16 have the same shape as the charge density vs. position (at any instant), according to equation I-3. The abscissa could be multiplied by 23 cm/360° to effect the change. For the purpose of calculating, the distribution-in-phase will do just as well as the distribution-in-position.

The height of the curves was tabulated at 1° intervals from 1° to 360°. (The height from 90° to 360° was always zero). These are tabulated in Tables I-7 to I-10. Then a cosine-sine numerical Fourier analysis was performed. The area under each curve is given by

$$C_o = \frac{1}{360} \sum_{i=1}^{360} y_i \qquad \text{(I-46)}$$

and the Fourier coefficients of the cosine and sine terms are given by

$$A_N = \frac{1}{180} \sum_{N=1}^{360} y_i \cos \frac{2\pi}{360} (iN) \qquad \text{(I-47)}$$

TABLE I-3 CASE NO. 1

(a)	(b)	(c)	(d)	(e)	(f)	(g)	(h)	(i)	(j)	(k)	(l)	(m)
1.00	23.8	20.8	0.67	42.1	.74	0.27	0	0.05	0	0	---	---
1.05	25.0	22.0	0.69	43.6	.72	0.28	.25	0.05	0.0100	0.0100	0.01	0.00145
1.10	26.3	23.3	0.74	47.3	.67	0.30	.50	0.05	0.0188	0.0128	0.02	0.00128
1.15	27.5	24.7	0.78	51.2	.62	0.32	.80	0.05	0.0291	0.0182	0.03	0.00182
1.20	28.6	25.6	0.81	54.1	.58	0.33	1.4	0.17	0.0489	0.0286	0.05	0.00286
1.25	29.8	26.8	0.84	57.1	.54	0.37	3.0	0.17	0.1010	0.0550	0.10	0.00548
1.30	31.0	28.0	0.88	61.6	.49	0.41	4.0	0.50	0.129	0.0665	0.13	0.00632
1.35	32.2	29.2	0.92	66.9	.42	0.48	2.0	0.17	0.062	0.0263	0.06	0.00262
1.40	33.5	30.5	0.96	73.8	.30	0.67	0.2	0.05	0.006	0.00179	0.01	0.00018
1.45	34.7	31.7	1.00	90°	0	----	0	0.05	0.000		0	-------

TABLE I-4 CASE NO. 2

(a)	(b)	(c)	(d)	(e)	(f)	(g)	(h)	(i)	(j)	(k)	(l)	(m)
1.00	23.8	20.8	0.63	39.0	0.77	.26	0	0.05	0	0	--	---
1.05	25.0	22.0	0.67	42.1	0.74	.27	.05	0.05	.0020	0.00149	1	0.00149
1.10	26.3	23.3	0.71	45.2	0.70	.29	0.15	0.05	.00575	0.00406	.33	0.00134
1.15	27.5	24.5	0.75	48.6	0.66	.30	0.25	0.05	.00910	0.00600	.20	0.00120
1.20	28.6	25.6	0.78	51.2	0.63	.32	0.40	0.05	.0140	.00880	.12	0.00105
1.25	29.8	26.8	0.82	55.1	0.57	.35	0.70	0.05	.0234	.01335	.07	0.000935
1.30	31.0	28.0	0.85	58.2	0.53	.38	3.75	0.50	.120	.06330	.13	.00825
1.35	32.0	29.2	0.89	62.9	0.46	.44	2.75	0.17	0.085	.0388	.06	.00232
1.40	33.5	30.5	0.93	68.4	0.37	.54	1.60	0.17	0.047	.0123	.11	0.00190
1.45	34.7	31.7	0.97	75.9	0.24	.84	0.10	0.05	.0029	.00705	.50	0.00352
1.50	35.8	32.8	1.00	90°	0	--	0	0.05	0	0	--	-----

TABLE I-5 CASE NO. 3

(a)	(b)	(c)	(d)	(e)	(f)	(g)	(h)	(i)	(j)	(k)	(l)	(m)
1.00	23.8	20.8	0.63	39.0	0.77	0.26	0	0.05	0	0	--	--
1.05	25.0	22.0	0.67	42.1	0.74	0.27	0.20	0.05	0.0080	0.0059	0.25	0.00197
1.10	26.3	23.3	0.71	45.2	0.70	0.29	0.30	0.05	0.0114	0.00805	0.16	0.00129
1.15	27.5	24.5	0.75	48.6	0.66	0.30	0.50	0.05	0.0182	0.0121	0.10	0.00121
1.20	28.6	25.6	0.78	51.2	0.63	0.32	0.75	0.05	0.0262	0.0164	0.04	0.00065
1.25	29.8	26.8	0.82	55.1	0.57	0.35	1.45	0.17	0.0487	0.0278	0.12	0.00333
1.30	31.0	28.0	0.85	58.2	0.53	0.38	2.10	0.17	0.0680	0.0357	0.08	0.00289
1.35	32.2	29.2	0.89	62.9	0.46	0.44	4.00	0.50	0.1250	0.0570	0.125	0.00712
1.40	33.5	30.5	0.93	68.4	0.37	0.54	0.75	0.05	0.0225	0.00828	0.067	0.00055
1.45	34.7	31.7	0.97	75.9	0.24	0.84	0.25	0.05	0.0073	0.00177	0.25	0.000442
1.50	35.8	32.8	1.00	90°	0	--	0	0.05	0	---	--	--

TABLE I-6 CASE NO. 9

(a)	(b)	(c)	(d)	(e)	(f)	(g)	(h)	(i)	(j)	(k)	(l)	(m)
0.80	19.1	16.1	.046	27.4	.89	0.22	0	0.05	0	0	--	--
0.85	20.3	17.3	0.49	29.4	.87	0.23	--	0.05	--	--	--	--
0.90	21.5	18.5	0.53	32.0	.85	0.24	0.50	0.05	0.0232	0.01967	0.10	0.001967
0.95	22.6	19.6	0.56	34.0	.83	0.24	--	0.05	--	--	--	--
1.00	23.8	20.8	0.59	36.2	.81	0.25	1.00	0.05	0.0421	0.0340	0.05	0.00170
1.05	25.0	22.0	0.62	38.7	.78	0.26	1.50	0.17	0.0600	0.04686	0.11	0.00528
1.10	26.3	23.3	0.66	41.3	.75	0.27	4.00	0.50	0.151	0.11340	0.12	0.0136
1.15	27.5	24.5	0.70	44.4	.71	0.28	8.00	0.50	.290	0.20706	0.06	0.01246
1.20	28.6	25.6	0.73	46.9	.68	0.29	10.00	0.50	.350	0.23940	00.05	0.0119
1.25	29.8	26.8	0.76	49.5	.65	0.31	2.10	0.17	.725	0.47052	0.08	0.0376
1.30	31.0	28.0	0.80	53.2	.60	0.33	0.60	0.05	.194	.011659	0.08	0.0093
1.35	32.2	29.2	0.83	56.1	.56	0.37	0.40	0.05	.124	0.06919	0.12	0.0083
1.40	33.5	30.5	0.87	60.5	.49	0.41	0.30	0.05	.090	0.04437	0.16	0.00709
1.45	34.7	31.7	0.91	65.5	.42	0.48	0.25	0.05	.072	0.030096	0.20	0.0060
1.50	35.8	32.8	0.93	68.4	.37	0.54	0.20	0.05	.057	0.02097	0.25	0.00524
1.55	37.0	34.0	0.97	76.0	.24	0.83	--	0.05	--	---	--	---
1.60	38.1	35.1	1.00	90°	0	--	--	0.05	0	0	--	---

TABLE I-7 CASE NO. 1

i	y_i	i	y_i	i	y_i	i	y_i
1-39	0	53	2.40	67	2.40	81	.05
40	.15	54	2.95	68	1.80	82	.05
41	.25	55	3.45	69	1.40	83	.05
42	.35	56	4.15	70	1.10	84	.05
43	.45	57	5.50	71	.80	85	0
44	.60	58	6.10	72	.60	86	0
45	.75	59	6.60	73	.40	87	0
46	.85	60	6.85	74	.30	88	0
47	1.00	61	6.95	75	.25	89	0
48	1.20	62	6.85	76	.20	90	0
49	1.35	63	6.55	77	.15	91-360	0
50	1.55	64	5.50	78	.10		
51	1.80	65	3.85	79	.10		
52	2.05	66	2.95	80	.10		

TABLE I-8 CASE NO. 2

i	y_i	i	y_i	i	y_i
1-40	0	57	4.50	74	.40
41	.05	58	6.30	75	.30
42	.10	59	6.10	76	.20
43	.15	60	5.45	77	.10
44	.20	61	4.90	78	.05
45	.25	62	4.25	79	.05
46	.30	63	3.65	80	0
47	.40	64	3.25	81	0
48	.45	65	2.80	82	0
49	.55	66	2.50	83	0
50	.65	67	2.15	84	0
51	.70	68	1.85	85	0
52	.80	69	1.60	86	0
53	.95	70	1.35	87	0
54	1.05	71	1.10	88	0
55	1.30	72	.85	89	0
56	2.75	73	.60	90-360	0

TABLE I-9 CASE NO. 3

i	y_i	i	y_i	i	y_i	i	y_i
1-38	0	53	2.05	68	1.10	83	.05
39	.10	54	2.25	69	.80	84	.05
40	.20	55	2.50	70	.55	85	0
41	.30	56	2.75	71	.45	86	0
42	.40	57	3.00	72	.35	87	0
43	.50	58	3.35	73	.30	88	0
44	.65	59	3.80	74	.25	89	0
45	.75	60	9.75	75	.20	90-360	0
46	.90	61	5.85	76	.15		
47	1.00	62	6.00	77	.15		
48	1.15	63	5.70	78	.15		
49	1.30	64	4.50	79	.10		
50	1.50	65	3.35	80	.10		
51	1.65	66	2.45	81	.10		
52	1.85	67	1.55	82	.10		

TABLE I-10 CASE NO. 9

i	y_i	i	y_i	i	y_i	i	y_i
0-27	0	44	1.90	61	.40	78	.25
28	.05	45	2.35	62	.35	79	.25
29	.05	46	2.85	63	.35	80	.25
30	.05	47	3.50	64	.30	81	.20
31	.05	48	4.15	65	.30	82	.20
32	.05	49	5.15	66	.30	83	.20
33	.10	50	4.60	67	.30	84	.20
34	.15	51	3.90	68	.25	85	.15
35	.20	52	2.40	69	.25	86	.15
36	.25	53	1.40	70	.25	87	.10
37	.35	54	.95	71	.25	88	.10
38	.40	55	.75	72	.25	89	.05
39	.60	56	.65	73	.25	90-360	0
40	.80	57	.55	74	.25		
41	1.00	58	.50	75	.25		
42	1.25	59	.45	76	.25		
43	1.60	60	.40	77	.25		

TABLE I-11 CASE NO. 1

N	$\lvert\eta_N\rvert$	N	$\lvert\eta_N\rvert$
1	1.00	17	0.29
2	0.98	18	0.26
3	0.95	19	0.24
4	0.91	20	0.23
5	0.86	21	0.21
6	0.81	22	0.19
7	0.75	23	0.18
8	0.69	24	0.16
9	0.63	25	0.14
10	0.57	26	0.13
11	0.52	27	0.12
12	0.46	28	0.10
13	0.42	29	0.09
14	0.38	30	0.08
15	0.34	31	0.07
16	0.31	32	0.06

TABLE I-12 CASE NO. 2

N	$\lvert\eta_N\rvert$	N	$\lvert\eta_N\rvert$
1	1.00	17	0.32
2	0.98	18	0.29
3	0.96	19	0.27
4	0.92	20	0.27
5	0.88	21	0.24
6	0.84	22	0.23
7	0.78	23	0.22
8	0.73	24	0.22
9	0.68	25	0.21
10	0.62	26	0.20
11	0.56	27	0.20
12	0.52	28	0.20
13	0.47	29	0.19
14	0.42	30	0.18
15	0.38	31	0.17
16	0.35	32	0.16

TABLE I-13 CASE NO. 3

N	$\lvert\eta_N\rvert$	N	$\lvert\eta_N\rvert$
1	1.0	17	0.28
2	0.9	18	0.27
3	0.9	19	0.26
4	0.9	20	0.25
5	0.8	21	0.24
6	0.7	22	0.23
7	0.7	23	0.22
8	0.6	24	0.20
9	0.5	25	0.19
10	0.5	26	0.18
11	0.4	27	0.17
12	0.4	28	0.15
13	0.3	29	0.15
14	0.3	30	0.14
15	0.3	31	0.13
16	0.3	32	0.13

TABLE I-14 CASE NO. 9

N	$\lvert\eta_N\rvert$	N	$\lvert\eta_N\rvert$
1	0.99	17	0.37
2	0.94	18	0.36
3	0.88	19	0.33
4	0.80	20	0.32
5	0.74	21	0.30
6	0.68	22	0.29
7	0.64	23	0.27
8	0.62	24	0.24
9	0.61	25	0.23
10	0.59	26	0.22
11	0.57	27	0.21
12	0.53	28	0.20
13	0.50	29	0.20
14	0.46	30	0.19
15	0.42	31	0.18
16	0.39	32	0.17

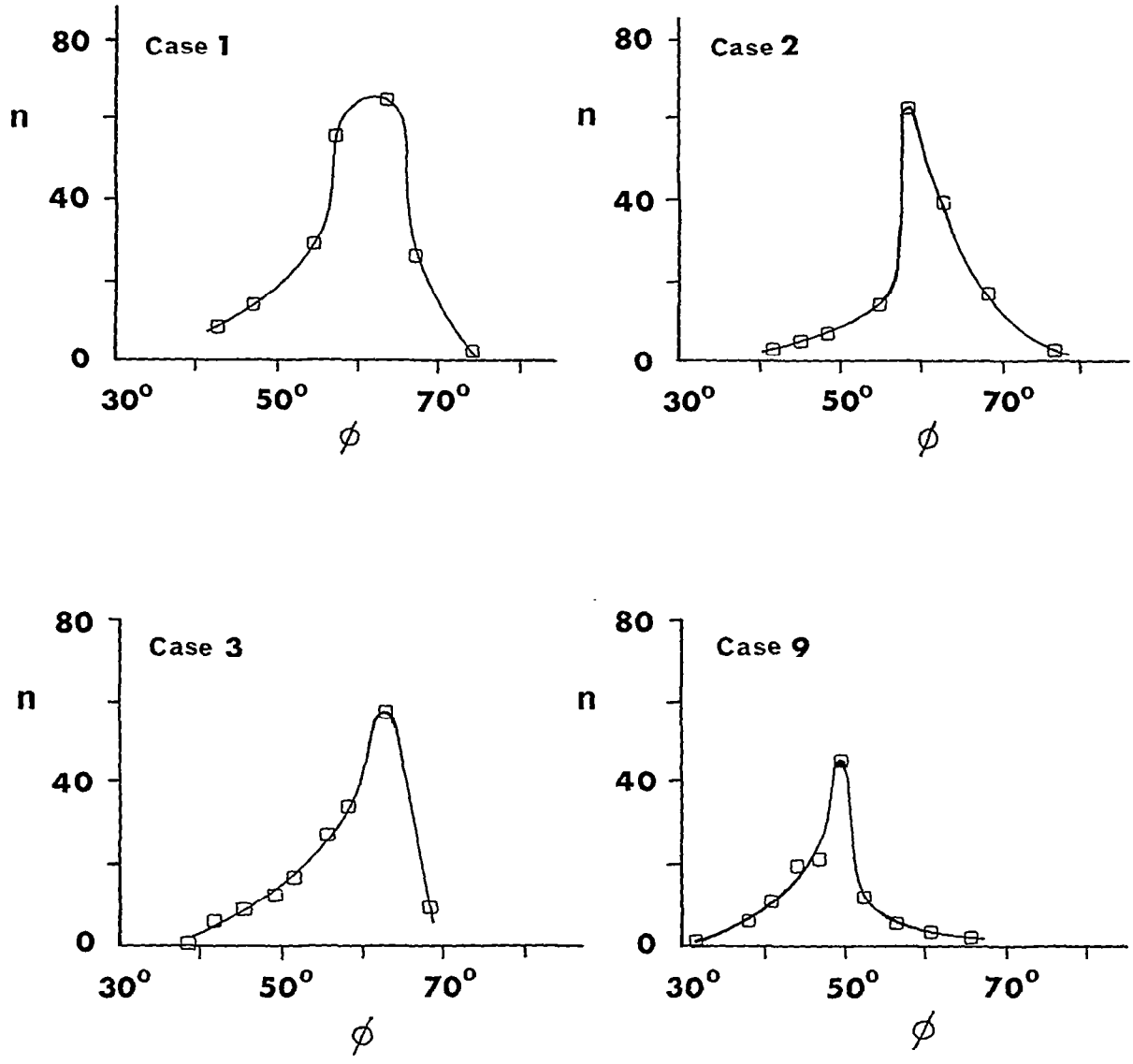

Actual phase distributions of electrons in a bunch as calculated from the undivided energy spectrum.

Figure 16

$$B_N = \frac{1}{180} \sum_{N=1}^{360} y_i \sin \frac{2\pi}{360} (iN) \qquad \text{(I-48)}$$

The coefficients were evaluated for the first 32 harmonics. Then the absolute value of the Fourier coefficient of an exponential series was calculated from

$$\left|C_N\right| = (A_N^2 + B_N^2)^{1/2} \tag{I-49}$$

Finally,

$$\left|\eta_N\right| = \frac{|C_N|}{2C_o} \tag{I-50}$$

The $\left|\eta_N\right|$ are listed in Tables I-11 to I-14.

Comments and Conclusions

The values of $\left|\eta_{16}\right|$ (equation 1) for the four cases are 0.31, 0.35, 0.30 and 0.39. Thus the Linac beam can be said to have a substantial sixteenth harmonic content.

The phase distributions of Figure 16 were calculated on the assumption that electrons become synchronous with the wave at 3 Mev. Slightly larger or smaller values might have been used and would have resulted in slightly different values of $\left|\eta_{16}\right|$. However, it is known from experience that the difference would not have been enough to reduce by an order of magnitude or more. It is safe to say that $\left|\eta_{16}\right|$ is in the neighborhood of 0.3.

In section 5 it was assumed that the rearmost electron in the bunch rides very close to the peak of the wave, so that in equation I-4 $\sin\phi_2 = 1$. Selecting a smaller value of $\sin\phi_2$ would have resulted in a narrower phase distribution and a larger value of $\left|\eta_{16}\right|$.

The Linac beam charge density for the sixteenth harmonic is

$$\hat{\rho}_{16} = \frac{q}{\pi a^2 v_b T}\ \eta_{16} \exp\ i\omega_{16}(z-v_b t)/v_b \tag{I-51}$$

This is the average density. The beam is actually densest on its axis. The density on the axis is approximately twice the average density. When the peak beam current is 0.3 A the charge per bunch is

$$\frac{0.3\ \text{A}}{1.3 \times 10^9/\text{sec}} = 2.3 \times 10^{10}\ \text{coulomb}$$

Also

$$\left|\eta_{16}\right| = 0.3, \quad \pi a^2 = 2 \times 10^{-4}\ \text{m}^2, \quad v_b T = 0.23\ \text{m}$$

so that

$$\left|\hat{\rho}_{16}\right| = 1.5 \times 10^{-6}\ \frac{\text{coul}}{\text{m}^3} \tag{I-52}$$

REFERENCES

1. D. Bohm and E. P. Gross, "Theory of Plasma Oscillations", Phys. Rev., 75, 1851-1876 (1949).

2. H. J. Merrill and H. W. Webb, "Electron Scattering and Plasma Oscillations", Phys. Rev., 55, 1191-1198 (1939).

3. D. H. Looney and S. C. Brown, "The Excitation of Plasma Oscillations", Phys. Rev., 93, 965-969 (1954).

4. S. Kojima and S. Hagiwara, "Radiation of Plasma Oscillations", J. Phys. Soc. of Japan, 15, 1904 (1960).

5. S. Kojima, K. Kato, and S. Hagiwara, "Oscillations in Plasma", J. Phys. Soc. of Japan, 12, 1276-1281 (1957). ibid 14, 821-827 (1959).

   S. Kojima, Private Communication, (1963).

   I. F. Kharchenko, Ya. B. Fainberg, R. M. Nikolaev, E. A. Kornilov, E. A. Lutsenko and N. S. Pedenko, Sov. Phys. JETP, 11, 493-498 (1960).

6. M. H. Cohen, "Radiation in a Plasma. I. Cerenkov Effect," Phys. Rev., 123, 711-721 (1961).

7. L. B. Loeb, "Basic Processes of Gaseous Electronics", Univ. of California Press, Berkeley (1960).

8. R. A. Demirkhanov, A. K. Gevorkov, and A. F. Popov, "Interaction of a Beam of Charged Particles with a Plasma", Sov. Phys. Tech. Phys., 5, 290-294 (1960).

9. E. R. Gaerttner, M. L. Yeater, and R. R. Fullwood, R. P. I. Linac Facility, Proceedings of the Neutron Physics Symposium, Academic Press, (1961).

10. S. C. Brown and W. P. Allis, Amer. Instit. of Phys. Handbook, p. 174, McGraw-Hill, New York (1957).

11. L. Spitzer, "The Physics of Fully Ionized Gases", Interscience Press, New York, (1956).

12. M. Chodorow, et al., "Stanford High Energy Linear Accelerator (Mark III)", Rev. Sci. Instr., 26, 134-204 (1955).

NASA-Langley, 1967 —— 25 CR-819